

Interim Report
for the period
May 1988 to
August 1989

Mechanisms of Chemical Vapor Deposition on Carbon Fibers

DTIC
ELECTE
DEC 19 1990
S B D
Co

October 1990

Author:
I.M.K. Ismail

University of Dayton Research Institute
300 College Park
Dayton OH 45469-0001

F04611-88-C-0020
UDR-TR-89-79

Approved for Public Release

Distribution is unlimited. The AL Technical Services Office has reviewed this report, and it is releasable to the National Technical Information Service, where it will be available to the general public, including foreign nationals.

Prepared for the: **Astronautics Laboratory (AFSC)**
Air Force Space Technology Center
Space Systems Division
Air Force Systems Command
Edwards AFB CA 93523-5000

NOTICE

When U. S. Government drawings, specifications, or other data are used for any purpose other than a definitely related Government procurement operation, the fact that the Government may have formulated, furnished, or in any way supplied the said drawings, specifications, or other data, is not to be regarded by implication or otherwise, or in any way licensing the holder or any other person or corporation, or conveying any rights or permission to manufacture, use or sell any patented invention that may be related thereto.


FOREWORD

This interim report was submitted by University of Dayton Research Institute, on-site contractor, on contract F04611-88-C-0020 with the Astronautics Laboratory (AFSC), Edwards AFB CA 93523-5000. AL Project Manager was Dr Wes Hoffman.

This report has been reviewed and is approved for release and distribution in accordance with the distribution statement on the cover and on the DD Form 1473.



WESLEY P. HOFFMAN
Project Manager



WAYNE E. ROE
Research Coordinator

FOR THE DIRECTOR



WILBUR W. WELLS
Technical Director
Propulsion Division

REPORT DOCUMENTATION PAGE

Form Approved
OMB No. 0704-0188

1. REPORT SECURITY CLASSIFICATION UNCLASSIFIED		1b. RESTRICTIVE MARKINGS	
2. SECURITY CLASSIFICATION AUTHORITY		3. DISTRIBUTION / AVAILABILITY OF REPORT Approved for Public Release; Distribution is unlimited.	
4. DECLASSIFICATION / DOWNGRADING SCHEDULE			
PERFORMING ORGANIZATION REPORT NUMBER(S) UDR-TR-89-79		5. MONITORING ORGANIZATION REPORT NUMBER(S) AL-TR-89-079	
6a. NAME OF PERFORMING ORGANIZATION University of Dayton Research Institute	6b. OFFICE SYMBOL (if applicable) UDRI	7a. NAME OF MONITORING ORGANIZATION Astronautics Laboratory (AFSC)	
8. ADDRESS (City, State, and ZIP Code) 300 College Park Dayton, Ohio 45469-0001		7b. ADDRESS (City, State, and ZIP Code) AL/RKPB Edwards AFB, CA 93523-5000	
9. NAME OF FUNDING / SPONSORING ORGANIZATION	8b. OFFICE SYMBOL (if applicable)	9. PROCUREMENT INSTRUMENT IDENTIFICATION NUMBER F04611-88-C-0020	
10. ADDRESS (City, State, and ZIP Code)		10. SOURCE OF FUNDING NUMBERS	
		PROGRAM ELEMENT NO. 61102F	PROJECT NO. 2306
		TASK NO. M1	WORK UNIT ACCESSION NO. E8

11. TITLE (Include Security Classification).

Mechanisms of Chemical Vapor Deposition on Carbon Fibers

12. PERSONAL AUTHOR(S)
Ismail M. K. Ismail

13a. TYPE OF REPORT Interim	13b. TIME COVERED FROM 88/5 TO 89/8	14. DATE OF REPORT (Year, Month, Day) 9010	15. PAGE COUNT 44
--------------------------------	--	---	----------------------

16. SUPPLEMENTARY NOTATION

COSATI CODES			18. SUBJECT TERMS (Continue on reverse if necessary and identify by block number) CVD, chemical vapor depositions, pyrolytic carbon, carbon fibers, carbon-carbon composites, pyrolysis, hydrocarbon cracking, surface properties.
FIELD	GROUP	SUB-GROUP	
21	08		
11	04		

19. ABSTRACT (Continue on reverse if necessary and identify by block number)

Deposition of pyrolytic carbon on the surface of carbon substrates, including carbon fibers, was studied at 1000-1100 C using two different systems, a static reactor operating at subambient pressures and a flow reactor operating at atmospheric pressure. The experimental parameters that affect the deposition rates and mechanism are substrate temperature, type of reactor used, total and partial pressure of methane in the static reactor, partial pressure of methane in the flow reactor, flow rate of hydrocarbon above substrate, presence of hydrogen in the deposition medium, and the type of substrate, as well as its surface area. (continued on next page)

→ next page

20. DISTRIBUTION / AVAILABILITY OF ABSTRACT <input checked="" type="checkbox"/> UNCLASSIFIED/UNLIMITED <input type="checkbox"/> SAME AS RPT. <input type="checkbox"/> DTIC USERS		21. ABSTRACT SECURITY CLASSIFICATION UNCLASSIFIED	
22a. NAME OF RESPONSIBLE INDIVIDUAL Dr. W. P. Hoffman		22b. TELEPHONE (Include Area Code) (805) 275-5306	22c. OFFICE SYMBOL RKPB

19. ABSTRACT (continued)

The two main differences between the deposition under flow and static conditions are rates of deposition and characteristics of deposits. While the rate under flow conditions is considerably higher than under static conditions, the deposits in the flow reactor are intact and less porous than those prepared in the static reactor. This is attributed essentially to the presence of hydrogen in the static reactor which lowers the rates of deposition, prevents the growth of intermediate species to large planar molecules, and attacks the carbon deposits.

Since the efficiency of deposition in the static reactor is poor, and the deposits are porous, the deposition under flow conditions is more favorable. The order of reaction, with respect to the partial pressure of methane in the flow, is close to unity. The deposition rates are proportional to the starting surface area of the carbon substrate with the rates on ungraphitized being higher than on graphitized carbons. This is attributed to the presence of metallic impurities with ungraphitized carbons which may catalyze the deposition reaction.

In addition to the experimental parameters and the type of reactor used, the nature and type of substrate are also other important parameters that should be considered while preparing carbon-carbon composites. On a small surface area material, as is the case with most carbon fibers and fabrics, the reaction starts in the gas phase and the rate-determining step is the cleavage of the C-H bonds of the hydrocarbon molecules. The intermediate species formed in the gas phase grows larger while depositing on the substrate. Increasing the flow rate of hydrocarbon during the reaction decreases the deposition rate and reduces the amount of deposit. By contrast, for carbon substrates having a large surface area (e.g. 55-60 m²/g), the rate-determining step is the collision between hydrocarbon molecules and the surface with concurrent deposition of pyrolytic carbon. In this case, the deposition rate and the amount of deposit increase with increasing the flow rate of the gas above the substrate.

Accession For	
NTIS GRA&I	<input checked="" type="checkbox"/>
DTIC TAB	<input type="checkbox"/>
Unannounced	<input type="checkbox"/>
Justification	
By	
Distribution/	
Availability Codes	
Dist	Avail and/or Special
A-1	



TABLE OF CONTENTS

<u>Section</u>	<u>Page</u>
SUMMARY	vii
INTRODUCTION	1
EXPERIMENTAL	2
Deposition Apparatus-Static Reactor	2
Flow Reactors	3
Nitrogen and Krypton BET Surface Areas and Porosity	4
Sample Activation	5
Materials	6
RESULTS AND DISCUSSION	7
Deposition in Static Reactor	7
<u>Deposition on As-Received VSB-32 Fiber</u>	7
<u>Properties of Activated VSB-32 Fiber Samples</u>	9
<u>Deposition on VSB-32 Activated Samples</u>	12
<u>Deposition on SP-1 Graphite Flakes</u>	16
Deposition in the Flow Reactor	18
<u>Effect of Temperature and Substrate on Deposition Rates</u>	18
<u>Pyrolytic Carbon Deposition on Carbon Fibers</u>	22
<u>Effect of Gas Composition</u>	24
<u>Effect of Flow Rate</u>	26
Properties of Deposits	27
<u>Deposits on VSB-32 Fibers</u>	27
<u>Deposits on V3G Carbon Black</u>	29
Mechanisms of Deposition	31
CONCLUSIONS AND RECOMMENDATIONS	32
REFERENCES	33

LIST OF FIGURES

<u>Figure</u>	<u>Caption</u>	<u>Page</u>
1	Static Reactor Used for CVD Studies.	2
2	Thermogravimetric Analyzer System Used for CVD Studies.	4
3	Schematic Diagram of Flow System Used for Preparing Larger Carbon-Carbon Composite Samples.	4
4	Dependence of Carbon Yields on Methane Partial Pressure in Static Reactor.	8
5	Comparison of Theoretical and Experimental CVD Carbon Yields.	9
6	Scanning Electron Micrographs of Graphitized VSB-32 Pitch Fiber	10
7	Dependence of Active Surface Area (ASA) on Level of Burn-Off.	11
8	Dependence of Total Surface Area on Burn-Off.	11
9	Dependence of ASA on Burn-Off After Deposition of One Layer of Pyrolytic Carbon.	13
10	Proposed Model for Crystallite Orientation in a Graphitized Pitch Carbon Fiber.	15
11	Scanning Electron Micrographs of SP-1 Graphite Before and After Deposition of Pyrolytic Carbon	19
12	Typical Thermograms for Methane Cracking Over VSB-32 Fiber (Flow System).	20
13	Dependence of CVD Rates on Reaction Temperature.	20
14	Variation of Activation Energy with Starting Surface Area.	21
15	Effect of Starting Surface on Deposition Rate (mg/g-min).	21
16	Effect of Starting Surface Area on Deposition Rate (mg/m ² -min).	23
17	Raw Data for the Deposition of Pyrolytic Carbon on Carbon Substrates at 1025 C.	23
18	Dependence of CVD Rates on Methane Concentration.	25
19	Dependence of Deposition Rate on Temperature (Arrhenius Plots) and Gas Composition.	25
20	Influence of Gas Flow Rate on Pyrolytic Carbon Deposition Rates.	26
21	Surface Area of Deposits Prepared in Flow and Static Reactor.	28

22	Scanning Electron Micrographs of VSB-32 Fiber Coated at 1273 K with 33% Pyrolytic Carbon: (a) and (c); Static Reactor, (b) and (d); Flow Reactor.	30
23	Surface Area of Carbon-Carbon Composites Prepared at 1025 C (Starting Substrate: V3G).	30
24	Proposed Mechanism of CVD in Static Reactor.	31
25	Proposed Mechanism of CVD in Flow Reactor.	32

LIST OF TABLES

<u>Table</u>	<u>Caption</u>	<u>Page</u>
1	List of Carbons and Their Surface Areas.	6
2	Properties of Pitch-Based Graphitized Fiber; VSB-32.	7
3	Active Surface Area (m^2/g) of Fiber Samples After Deposition of Several Pyrolytic Carbon Layers.	13
4	Total (BET) Surface Area of Fiber Samples Before and After Deposition of One Pyrolytic Carbon Layer.	14
5	Variation of ASA With the Number of CVD Layers Deposited on SP-1 Graphite Activated to 12.4% B.O.	16
6	ASA and Total BET Areas of SP-1 Graphite Sample Activated to 12.4% B.O.	17
7	X-ray Parameters of Carbon Fibers and SP-1.	24
8	Active Surface Area (ASA and Deposition Rates of Selected Carbons.	24

SUMMARY

Deposition of pyrolytic carbon during methane cracking on the surface of several carbon substrates, including carbon fibers, was studied at 1000-1100 C using two main systems: a static reactor operating at subambient pressures and a flow reactor operating at atmospheric pressure. The experimental parameters that affect the deposition rates and hence can alter the mechanism are temperature of substrate, type of reactor used, total and partial pressure of methane in the static reactor, partial pressure of methane in the flow reactor, flow rate of hydrocarbon above substrate, presence of hydrogen in the deposition medium, and the type of substrate as well as its surface area.

Under otherwise similar experimental conditions, the two main differences between the deposition under flow and static conditions are deposition rates and characteristics of deposits. While the rates under flow conditions are as much as five times higher than under static conditions, the deposits in the flow reactor are intact and less porous than those prepared in the static reactor. This is attributed essentially to the presence of hydrogen in the static reactor which acts as an inhibitor for the deposition reaction; it lowers the rates of deposition, prevents the growth of intermediate species to large planar molecules, and attacks the carbon deposits.

In the static reactor the efficiency of deposition is poor. As the starting partial pressure of methane, or total pressure of the system increases, the deposition rates are lowered and the efficiency is reduced even more.

On the other hand, the deposition under flow conditions is perhaps more favorable because the order of reaction, with respect to the partial pressure of methane in the flow, is close to unity. The deposition rates are proportional to the starting surface area of the carbon substrate and the rates on ungraphitized are higher than on graphitized carbons. This is attributed to the presence of metallic impurities with ungraphitized carbons which may catalyze the deposition reaction and also to the difference in structure between both categories of materials. The crystallites in graphitic materials are larger and more ordered than in ungraphitized carbons.

Although the experimental parameters and the type of reactor play a major role towards defining the mechanism of deposition, the nature and type of substrate are also important parameters. On a small surface area material, as is the case with carbon fibers and fabrics, the reaction starts in the gas phase and the rate-determining step is the cleavage of the C-H bonds of the hydrocarbon (activation energy ~100 kcal/mole). The intermediate species formed in the gas phase would grow larger while depositing on the substrate. Increasing the flow rate of hydrocarbon during the reaction decreases the deposition rate and reduces the amount of deposit. On the other hand, for carbon substrates having a large surface area (e.g. 55-60 m²/g), the rate - determining step is the collision between hydrocarbon molecules and the surface with concurrent deposition of pyrolytic carbon. In this case, the deposition rate and the amount of deposit increase with increasing flow rate of the gas above the substrate.

The results presented in this report were also used to propose a model describing the orientation of crystallites in the graphitized pitch VSB-32 fiber, and to propose two mechanisms for the chemical vapor deposition of pyrolytic carbon on the fiber. The outer crystallites are oriented in the circumferential direction, but the inner ones are oriented in the radial direction. Naturally between these two extremes, there is a region where the crystallites are randomly oriented.

INTRODUCTION

Carbon fiber reinforced carbon composites (C-C composites) are the state-of-the-art materials for numerous aerospace applications requiring high strength and modulus, light weight, and wear resistance. A C-C composite has normally two main components: a carbon fiber and a matrix. While the fiber imparts strength to the composite, the matrix holds the fiber bundles together. There are at least three major industrial methods for fabricating carbon composites: coal or petroleum tar impregnation, resin impregnation, and chemical vapor deposition (CVD).

With the first two processes, the fiber is normally impregnated with a matrix under given manufacturing conditions of temperature, pressure, and residence time. If the end product has low density, which means that the composite is highly porous, it undergoes successive densification cycles. To densify a composite and achieve the desired density, the composite is either subjected to successive impregnation, carbonization and high temperature graphitization cycles, or it is exposed to a hydrocarbon gas under conditions that permit the deposition of pyrolytic carbon inside the pores (infiltration).

C-C composites can also be prepared directly by the CVD process where pyrolytic carbon is deposited from the gas phase on a fiber substrate. In other words, a carbon fiber or fabric is first woven to yield a preform which is then exposed, under certain experimental conditions, to a hydrocarbon gas (or a mixture of a hydrocarbon and an inert gas) until the desired properties are reached. This process is simple and clean when compared to resin or coal-tar impregnation. However, although a considerable amount of research has been reported in the literature on the first two processes, little attention was given to the CVD process on carbon fibers and fabrics. The overall objective of the present work is to understand the mechanism(s) of deposition of pyrolytic carbon on different carbon substrates. The specific objectives are:

1. To elucidate how the experimental parameters (temperature, pressure, gas flow rate, and gas composition) can affect the deposition rates and possibly alter the deposition mechanism.
2. To investigate the differences between the mechanism of deposition under static and flow conditions.
3. To examine how the substrates may affect the properties of the end products such as their porosity, surface area, and morphology.
4. To examine how the starting properties of carbon substrates can influence the deposition mechanism.
5. To determine whether pyrolytic carbon deposits primarily on active or total surface area of substrates.
4. To propose, based on the generated data, the possible mechanisms associated with the CVD reaction on different carbon substrates.

EXPERIMENTAL

Two major experimental setups were used in the present study: a static reactor operating at subambient pressures, and a thermogravimetric analyzer (TGA) operating at ambient pressure under flow conditions. For surface area determinations, two automated Digisorb Instruments, 2500 and 2600, were used.

Deposition Apparatus-Static Reactor

Fig. 1 illustrates a schematic diagram of the entire system connected to the static reactor. The main components of the system are (1) a quartz reactor holding the sample placed in a quartz boat, (2) an induction furnace that can be heated to 1100 C, (3) a furnace controller, (4) a gas reservoir holding the hydrocarbon gas (methane), (5) several pumps used to evacuate the sample prior to the deposition reaction, (6) a mass-spectrometer connected to system manifold via a variable leak valve, and (7) a Zenith computer to control the operation, to save the data on diskettes, and to perform the required computations and analysis.

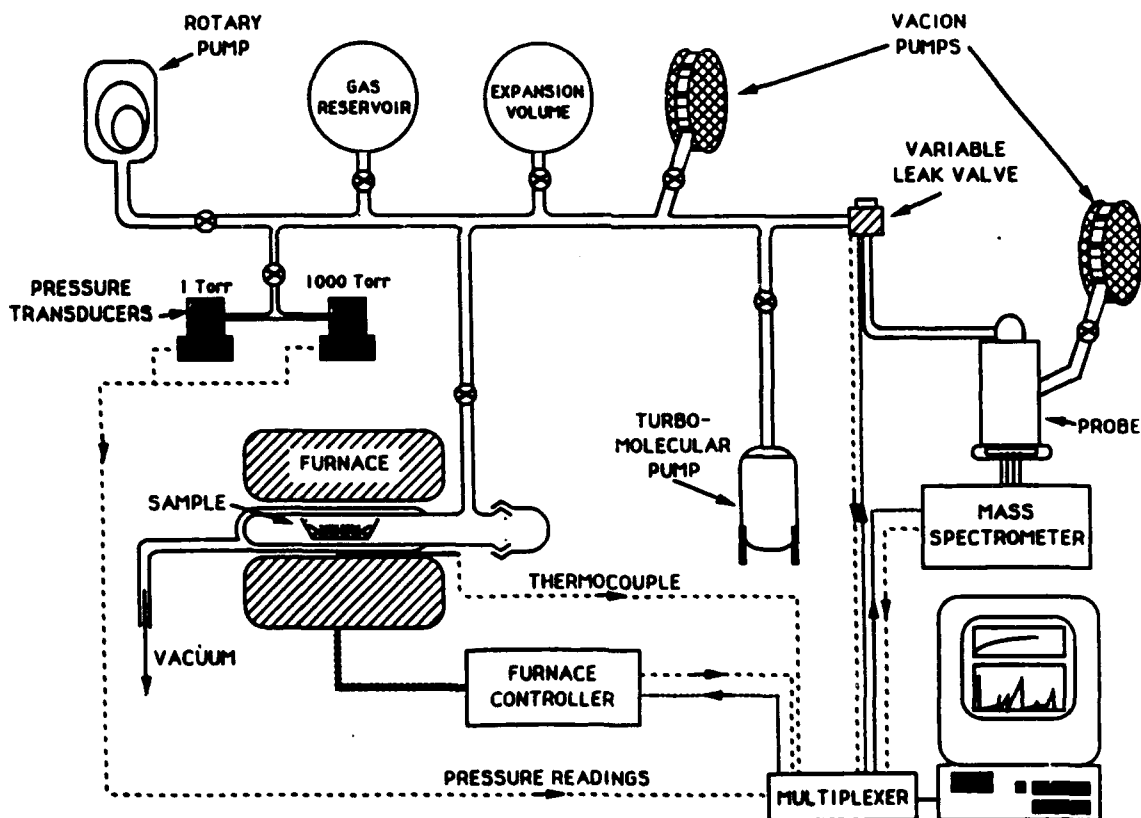


Figure 1. Static Reactor Used for CVD Studies.

The procedure adopted for these experiments may be summarized as follows. A known weight of a carbon substrate (carbon fiber or black) was placed in the quartz boat, evacuated for 2 h at 1000 C to 10^{-7} Torr, and finally exposed to one dose of methane at a starting pressure in the range of 1 - 200 Torr. As the reaction proceeded, mainly CH_4 yielding $2\text{H}_2 + \text{C}$, the pressure of the system increased and the concentration of methane decreased while that of hydrogen increased. Variation in gas concentration and system pressure was monitored for 15 h using the mass-spectrometer. After terminating a run and cooling to room temperature, the sample (carbon substrate with pyrolytic carbon deposits) and boat were weighed, and the amount of carbon deposited on each was calculated. "Blank" runs were also performed in the system where the empty boat was exposed to methane under conditions (pressure, temperature, and residence time) identical to those used in presence of carbon substrates. The amount of pyrolytic carbon deposit on the "bare" boat was then obtained.

Flow Reactors

For the experiments performed under flow conditions at ambient atmosphere, two experimental setups were used; a thermogravimetric analyzer (TGA) for measuring deposition rates on a few milligram sample, and a large quartz reactor for preparing sizeable composites that could be further examined and characterized. With the TGA, a computerized Cahn-113 system (Fig. 2), a small sample (5-40mg) was suspended on the electrobalance, evacuated at room temperature to 10^{-5} Torr, flushed with ultrahigh purity nitrogen or argon to ambient pressure, heated to 1080 C under N_2 , cooled to a designated CVD temperature in the range of 1000-1080 C, and finally exposed to a flowing mixture of methane and argon at 150 cc/min. The percent of methane in the mixture was 2.7, 11.1, or 16.2%. The increase in sample weight due to the deposition was recorded. Blank runs were also executed on an empty sample container giving, in most cases, insignificant amounts of deposit.

The other large reactor, which was operating under conditions simulating those of the TGA system, is shown in Fig. 3. Based on the results obtained with the TGA system, the operating parameters were chosen to prepare selected C-C composite samples. A known weight of the substrate (2-3 g) was placed in the reactor, evacuated, flushed with an inert gas (Ar or N_2), and heated to a designated temperature (1000-1050 C). After holding the sample at the isothermal temperature for 30 minutes, a mixture of 10% methane in argon was flowed over the sample at 150 cc/min for a desired length of time or until the projected amount of carbon deposit was reached. The reactor was then cooled to room temperature under a flow of the inert gas, and the sample was pulled out for further testing.

Nitrogen and Krypton BET Surface Areas and Porosity

Two Digisorb instruments 2500 and 2600, manufactured by the Micromeritics Co. (Norcross, Georgia), were used to determine the BET areas and to obtain the adsorption/desorption isotherms required for pore size distribution analysis. The operation of this equipment is fully automated via computers. For all surface area determinations, a standard sample, SP-1 Graphite (BET area = $2.00 \text{ m}^2/\text{g}$), was used to confirm the validity of the data obtained on the unknown samples.

After a sample was properly outgassed at 150 C, it was cooled, then immersed in a liquid nitrogen bath (-196 C). A small dose of N_2 (or Kr) was admitted into the system. When an equilibration was attained, the equilibrium pressure, P , was noted, and the volume of gas, V (cc/g at STP), was computed. The sample was once again subjected to a

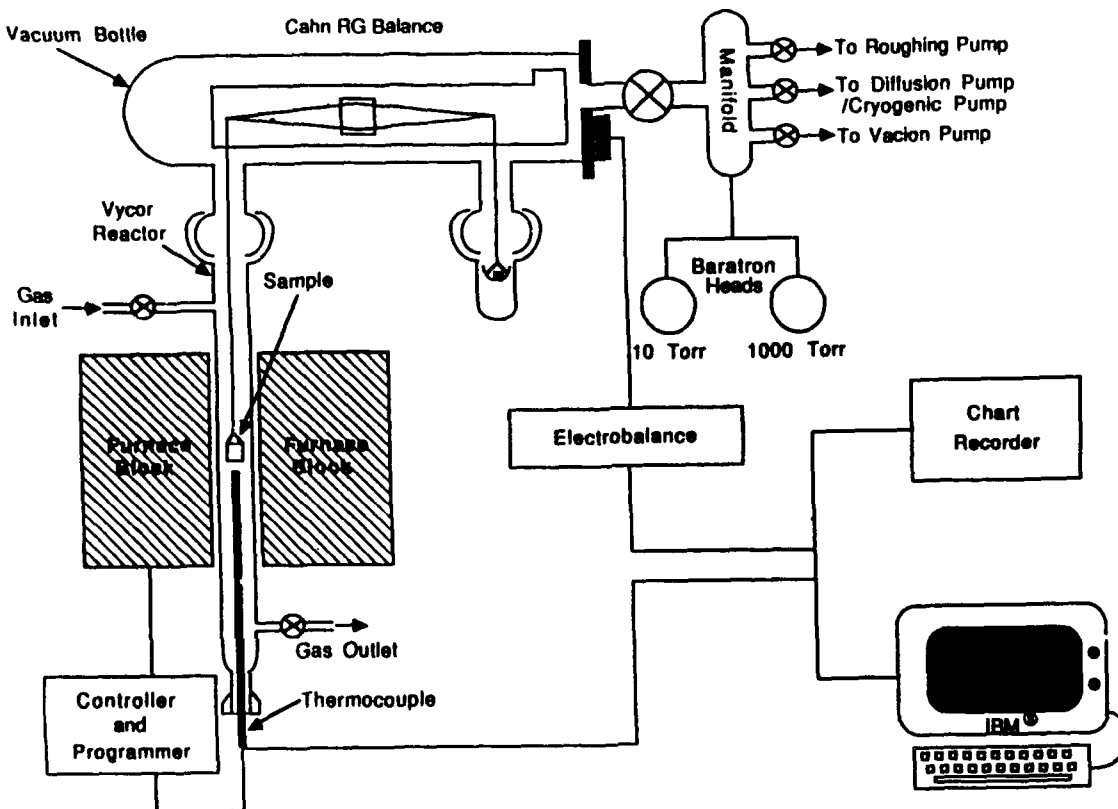


Figure 2. Thermogravimetric Analyzer System Used for CVD Studies.

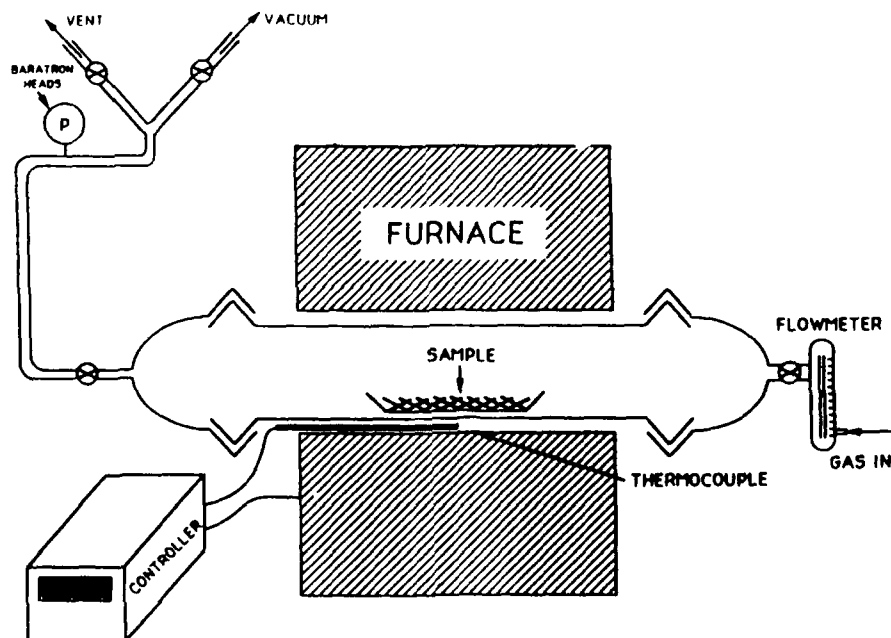


Figure 3. Schematic Diagram of Flow System Used for Preparing Larger Carbon-Carbon Composite Samples.

slightly higher pressure and the second values of P and V were determined. This step was repeated several times until the projected relative pressure values were reached (about 0.21 for surface area determinations and 0.985 for obtaining full isotherms). In the former case, a plot between P/P^0 and the term $P/V (P^0 - P)$ was made (where P^0 is the saturation pressure of adsorbate) to yield a straight line. The number of data points on each plot was at least five. The slope, S, and intercept, I, were used to calculate the monolayer volume, V_m , i.e., the volume of adsorbate required to cover the entire surface of one gram sample with one complete monolayer. The Brunauer, Emmett, and Teller (BET) equation was used to compute the monolayer volume (Ref. 1):

$$\frac{P}{V(P^0 - P)} = \frac{1}{V_m C} + \frac{C-1}{V_m C} \cdot \frac{P}{P^0} \quad (1)$$

$$V_m (\text{cc/g at STP}) = \frac{1}{S+I} \quad (2)$$

Assuming the cross-sectional area of nitrogen and krypton as $0.162 \text{ nm}^2/\text{molecule}$ and $0.180 \text{ nm}^2/\text{Kr atom}$, respectively, the total surface area (TSA) was calculated using:

$$\text{Nitrogen TSA (m}^2\text{/g)} = \frac{4.35}{S+I} = 4.35 V_m \quad (3)$$

$$\text{Krypton TSA (m}^2\text{/g)} = \frac{5.64}{S+I} = 5.64 V_m \quad (4)$$

It may be added that the value of 0.180 was obtained by calibration against nitrogen and that the saturation pressure of supercooled Krypton was used in the analysis as discussed elsewhere (Ref.2). This value corresponds to $0.214 \text{ nm}^2/\text{Kr atom}$ if the saturation pressure of solid Krypton, rather than the supercooled state, was used in the analysis (Ref. 2).

The data obtained with the full adsorption/desorption isotherms were also used to predict the type of pores present in the sample and also to estimate the pore volume and pore size distribution in the range 2.0 to 50.0 nm. Here, the adsorption measurements were continued to higher values of P/P^0 (up to $P/P^0 = 0.985$). The adsorption data, along with a simple mathematical model, were used to compute the pore volumes. The carbons, like many other porous materials, have cracks, crevices, and pores. Therefore, when exposed to an adsorbate (e.g. N_2), the pores are partially filled as a result of forming the monolayer and multilayers on top of it. The smaller pores will fill first with condensed N_2 molecules, and progressively the larger pores will fill afterwards as the equilibrium pressure is shifted to higher values. The experimental data collected, volume adsorbed vs. equilibrium pressure, can then be used with the model to execute a pore size distribution analysis. Details regarding these calculations have been described earlier (Ref. 3).

Sample Activation

Since CVD is a heterogeneous reaction, it is important to elucidate the role of different types of surfaces on deposition rates. When the hydrocarbon molecules in the gas phase collide with a substrate surface, they may collide with an active or nonactive site. The as-received fibers have small surface areas, and their contribution to the reaction is small. To improve the adhesion between the substrate and matrix, it was then desirable to modify the fiber surface and enhance its surface area. Surface modification of the fibers is

normally done by using some oxidation pretreatment procedures. In this study, two oxidation treatments, namely high - temperature oxidation (HTO) and low - temperature oxygen plasma etching (LTOPE) were used. The graphitized pitch carbon fiber, VSB-32 was used for this purpose. For preparing HTO activated samples, batches of the as-received fiber were oxidized in air inside a muffle furnace at an isothermal temperature of 500, 600, 700, or 925 C. The length of oxidation time at each temperature was varied until reasonable levels of burn-off (B.O.) were reached. LTOPE treatments were performed inside an RF oxygen plasma chamber operating under the following conditions: RF = 100 watts, flow rate = 100 cc/min, and chamber pressure = 67 Pa.

The active surface area (ASA) of all samples was determined by the oxygen chemisorption technique discussed earlier (Ref. 4). The chemisorption was carried out at 300 C and a starting oxygen pressure of 667 Pa and the two desorption cycles were executed at 950 C.

Materials

Several types of carbonaceous materials were used in this work; they are all listed in Table 1. The three carbon fibers were prepared from different precursors (rayon, pitch, and polyacrylonitrile) and heat treated to different temperatures. These are T-300, VSB-32, and WCA. SP-1 is a perfectly ordered graphitic material with an interlayer spacing of 0.3354 nm. ST MT and V3G are graphitized carbon with different particle sizes and surface areas; they have been heat treated to 2800 C. A portion of the V3G samples was activated in air to the 30% level of burn-off. As a result, new porosity was developed and both ASA and BET areas increased. The remaining five materials, N990, N762, N550, N330, and V3 are all ungraphitized carbon blacks.

TABLE 1. List of Carbons and Their Surface Areas.

Material	Type Of Carbon	Surface Area m ² /g
T-300	PAN ^{**} -Based Carbonized Fiber	0.56 [#]
WCA	Graphitized Rayon Fabric	0.66 [#]
VSB-32	Graphitized Pitch Fiber	0.54 [#]
SP-1	Spectroscopic Grade Graphite	2.00 [*]
N990	Ungraphitized Carbon Black	7.5 [*]
N762	Ungraphitized Carbon Black	25.5 [*]
N550	Ungraphitized Carbon Black	37.0 [*]
N330	Ungraphitized Carbon Black	80.2 [*]
V3	Ungraphitized Carbon Black	71.0 [*]
ST MT	Graphitized Carbon Black	9.1 [*]
V3G	Graphitized Carbon Black	59.2 [*]
V3G,30% B.O.	V3G Activated to 30% Burn-off	99.7 [*]

* Surface Areas Determined By N₂ Adsorption At -196 C

Surface Areas Determined By Kr Adsorption At -196 C

** Polyacrylonitrile

RESULTS AND DISCUSSION

Deposition in Static Reactor

Deposition on As-Received VSB-32 Fiber

In this section, the results obtained on the as-received graphitized pitch-based fiber, VSB-32, are reported. Table 2 summarizes some basic properties of this substrate. The small surface area, as measured by gas adsorption and the density values, which are in excess of 2.0 g/cc, indicates that this fiber has a small level of open and closed porosity. The results obtained for pyrolytic carbon deposition on the as-received fiber at 1000 C are shown in Fig. 4. The amount of deposit after 15 h exposure increases with the starting pressure of methane in the reactor. Curve A represents the total carbon yield calculated from the drop in methane concentration while curve W represents the increase in sample weight obtained by using an analytical balance. The difference between A and W gives the amount of carbon deposited on the boat and reactor walls. Line C shows the amount of deposit on the boat in the presence of fibers; this amount is constant above 60 Torr. Curve B exhibits the deposit on a bare boat ("Blank" runs) in absence of fiber. When compared to C, curve B is not only higher, but is also dependent on methane pressure. There are two possible reasons for this: (i) In the presence of the fiber, a portion of the boat surface is covered, and diffusion of methane to the internal surface of the boat is restricted. However, this reason is not enough to account for the large difference between curves B and C. (ii) Methane cracks preferentially over the carbon fiber surface. The general trend of curves A or W means that with increasing methane pressure, the amounts of deposit on fiber and of methane which has cracked in the gas phase increase at a decreasing rate.

TABLE 2. Properties of Pitch-Based Graphitized Fiber; VSB-32.

Diameter (nm)	10670
Number Of Filaments/Toe	2K
He-Density(g/cc)	2.113
Hg-Density(g/cc)	2.022
Density From Gradient Columns (g/cc)	2.037
Kr-BET Surface Area (m²/g)	0.540
Geometric Surface Area (m²/g)	0.180
Active Surface Area (m²/g)	0.029
Crystallite Parameters (nm):	
d002	0.3420
L_c	6.0
L_a	3.0
Ash (%)	<0.05
S (%)	0.64
H (%)	0.08
N(%)	0.007
Na (ppm)	4.4
K (ppm)	4.2
Ca, Zn, Fe, Mg	Not Detected

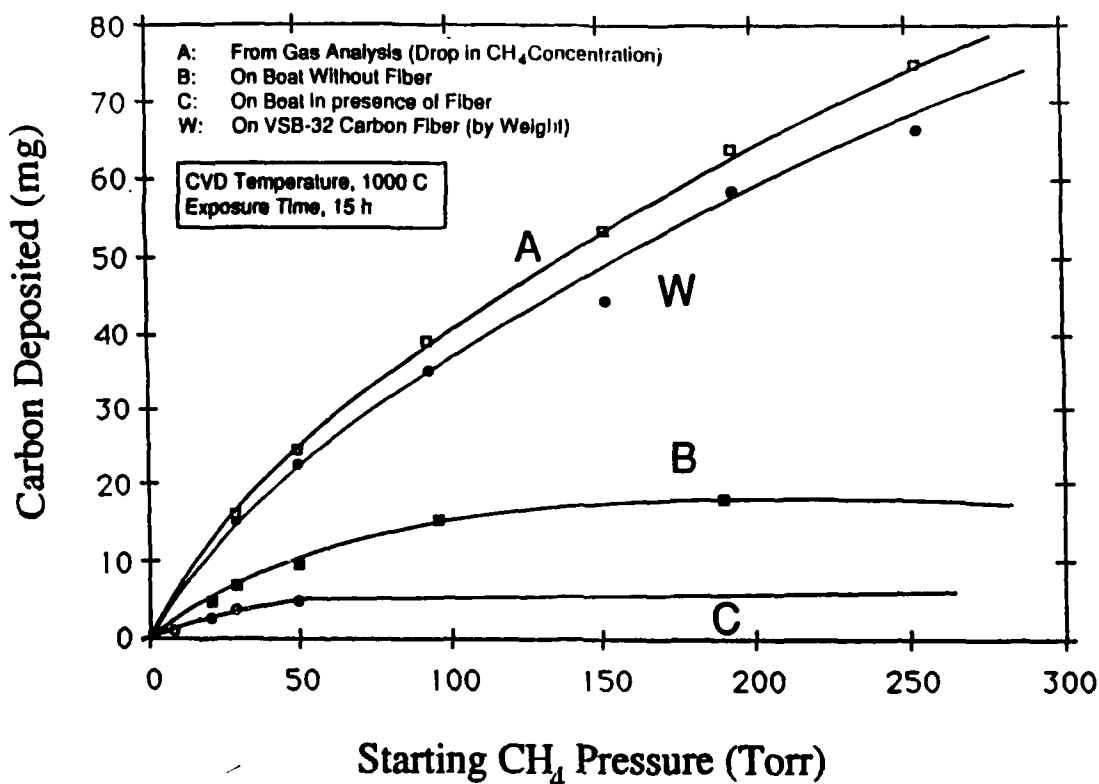


Figure 4. Dependence of Carbon Yields on Methane Partial Pressure in Static Reactor.

Next, we discuss the thermodynamic considerations (Fig. 5). Line T represents the yield of carbon that would have deposited if the actual thermodynamic equilibrium conditions at 1000 C had been reached. Curve W (from Fig. 4) displays the experimental values which are well below line T. It is evident that as the starting pressure of methane increases, the deviation from thermodynamic equilibrium becomes more pronounced and, therefore, the efficiency of utilizing methane in the deposition reaction becomes less. There are three main reasons for this: (i) Increasing the pressure shifts the equilibrium to unfavorable conditions, (i.e. recombination of carbon and H₂ to form CH₄). (ii) At higher pressures, the concentration of H₂ is high. It is possible that H₂ may retard methane cracking. (iii) Elevated pressures may enhance the rate of by-product condensation on fiber active sites. As a result, the rate of CVD drops due to the lack of active centers.

The effect of adding diluents to methane was also studied (curve D-Fig. 5). Here the fiber was exposed to a mixture of methane (starting pressure: 90-200 Torr) and either He or Ar. The diluent was added to give a total starting pressure of 500 Torr. It is seen from the figure that for any given value of methane pressure, the amount of deposit is higher in absence of diluents (compare plot W versus D). Thus, by increasing the total pressure in the system while maintaining a constant methane concentration, the CVD rate is retarded and the carbon yield decreases.

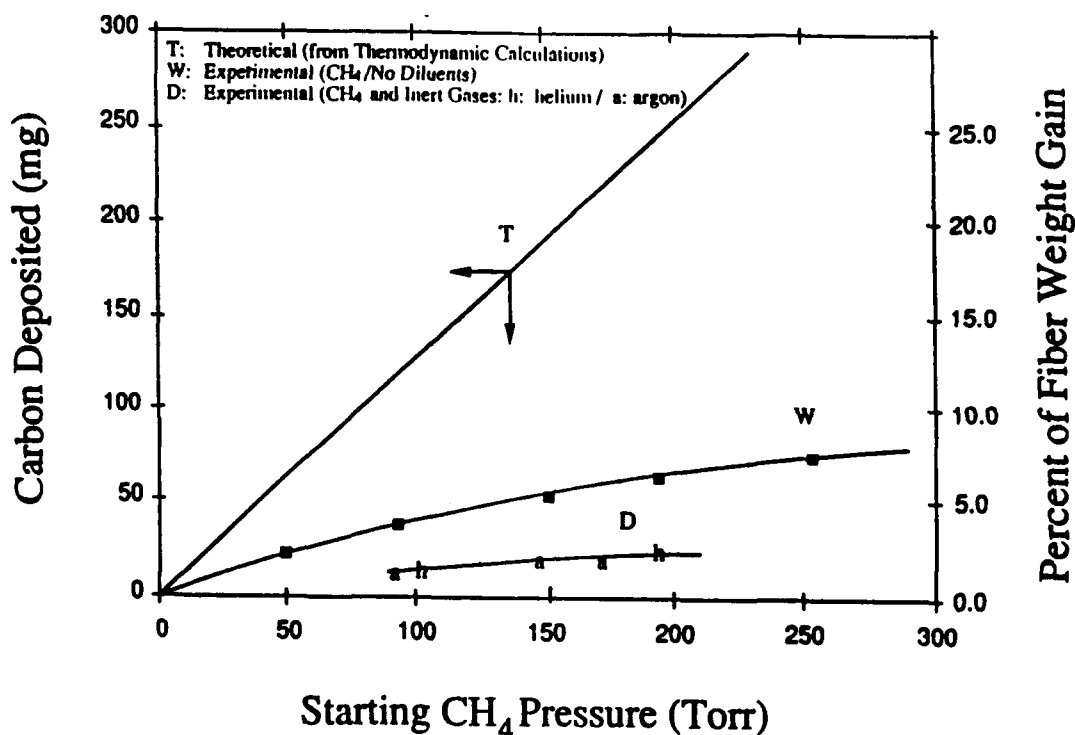


Figure 5. Comparison of Theoretical and Experimental CVD Carbon Yields.

Properties of Activated VSB-32 Fiber Samples

Scanning Electron Micrographs of different oxidized VSB-32 fiber samples are displayed in Fig. 6. The as-received fiber surface (plate a) has few striations and wrinkles. Oxidation in the plasma to 27% B.O. (plate b) and above, or in air at 500 C to 4.1% B.O. (plate c) only smoothed the surface but did not develop pits or pores. At higher levels of B.O. at 500 C, there was some indication of oxygen attacking the fiber through the ends and the oxidation process propagated inward in the filament axial direction. As a result, a few hollow "straw-like" tubes were seen (plate d). Oxidation at 600 and 700 C to 4% B.O. and above developed a considerable number of pits and holes along the filament side (plates e and f) whose depth and size increased with B.O. These observations indicate that oxidation of the graphitized pitch fiber can take place by more than one mechanism depending on the experimental parameters used (activation temperature, activation time, and type of oxidant gas).

Fig. 7 shows how the ASA of the activated samples changes with B.O. When the B.O. increases from 0 to about 1%, the ASA abruptly increases by a factor of 5 from a starting value of $0.029 \text{ m}^2/\text{g}$ for the as-received fiber to about $0.15 \text{ m}^2/\text{g}$. Oxidation of the samples to higher levels of B.O. is associated with a slight increase in ASA. Thus, between 1 and 80% B.O., the ASA is linearly related to B.O.; the slope of the line ($d\text{ASA}/d\%\text{B.O.}$) is mainly dependent on the treatment. At one extreme, all samples

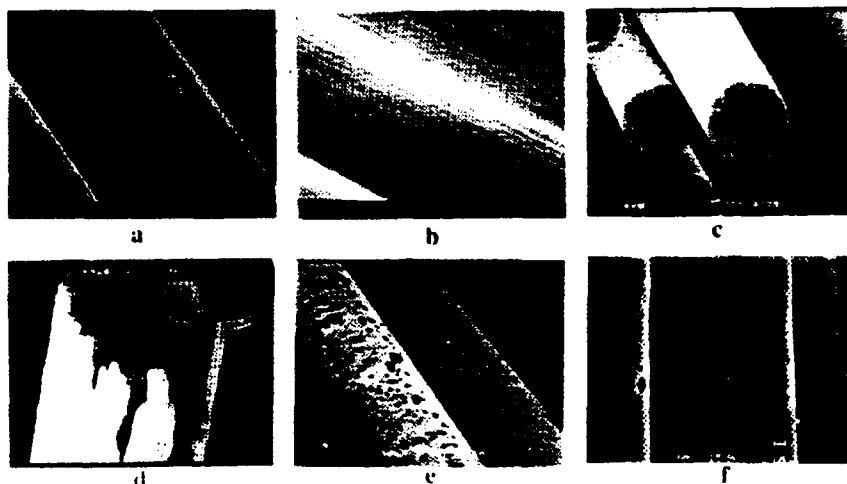


Figure 6. Scanning Electron Micrographs of Graphitized VSB-32 Pitch Fiber: a; As-Received Fiber, b; Activated in Oxygen Plasma to 27% B.O., c; Activated in Air at 500 C to 4.1% B.O., d; Activated in Air at 500 C to 57% B.O., e; Activated in Air at 600 C to 7.6% B.O., f; Activated in Air at 700 C to 4.6% B.O.

exposed to HTO of 600 C and above, exhibit one line having the lowest slope of $10 \text{ cm}^2/\text{g}/\% \text{B.O.}$ By contrast, the samples oxidized at 500 C gave the highest slope; $70 \text{ cm}^2/\text{g}/\% \text{B.O.}$ As Fig. 7 shows, the samples activated at 500 C have larger ASA than the corresponding ones activated to the same level of B.O. at 600-925 C. This finding indicates that there are, at least, two possible mechanisms for HTO. One is predominating at 500 C where the attack of oxygen molecules occurs mainly through the ends of the carbon filaments and progresses inward into the axial direction, while the other mechanism is predominating at the higher temperatures where the attack is primarily taking place at the sides of the filaments and is progressing into the radial direction towards the center of the filaments.

It is also noted in the figure that the LTOPE samples exhibit a line located between the above two extremes with a slope $= 32 \text{ cm}^2/\text{g}/\% \text{B.O.}$ Since the plasma generates several types of excited species including atomic oxygen, the etching in this case is probably due to the random attack at the basal planes and active sites with the removal of one graphitic layer after the other. In other words, because of the short residence time of the excited species, the probability of oxygen atoms to penetrate deeply below the surface is small. Since the depth of penetration is small, the formation of pits is not observed.

Variation of total (BET) surface area with B.O. is shown in Fig. 8. Below 25% B.O., the increase in total area with B.O. is linear and insignificant porosity has developed. As the B.O. increases above this level, the total area increases exponentially with B.O. because porosity starts developing considerably above this level. For the HTO samples, decreasing the activation temperature from 700 to 500 C is associated with an enhancement of the total area at a given B.O.

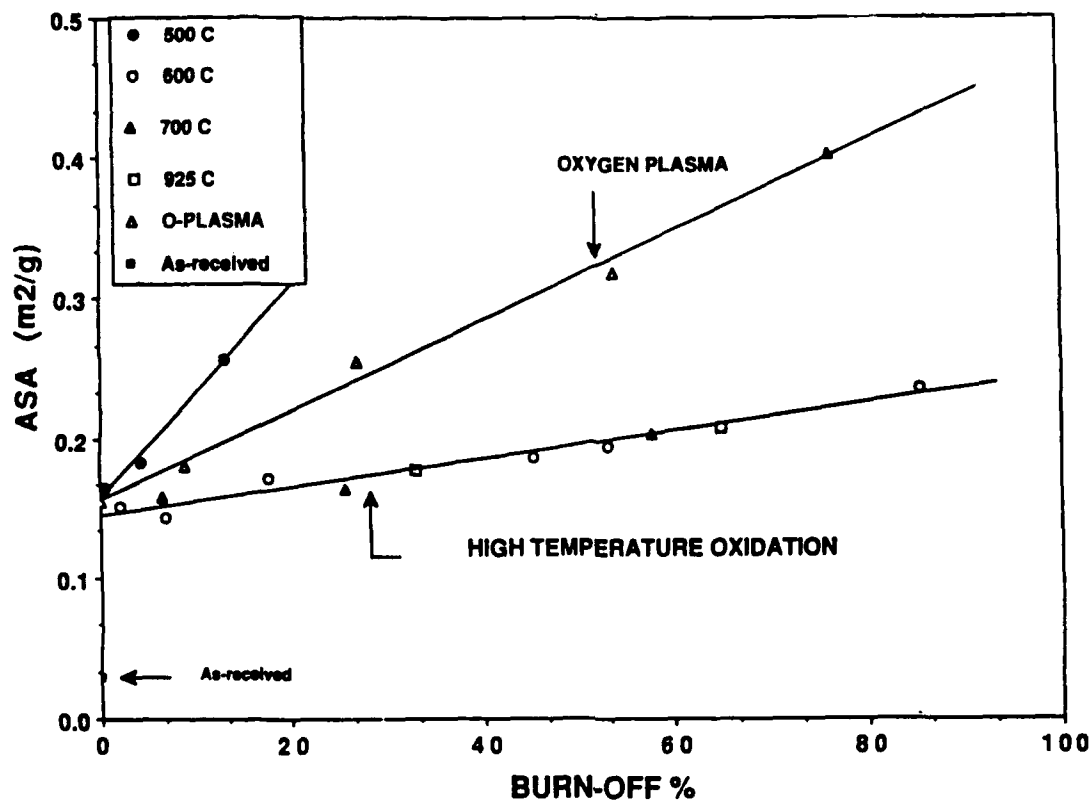


Figure 7. Dependence of Active Surface Area (ASA) on Level of Burn-Off.

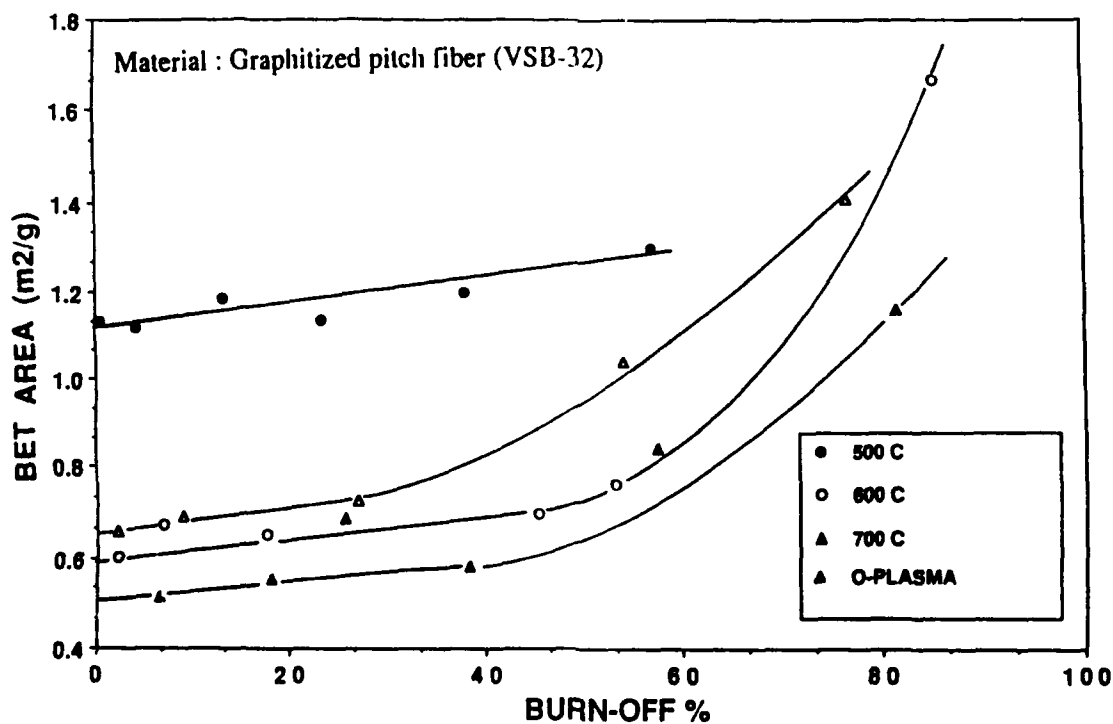


Figure 8. Dependence of Total Surface Area on Burn-Off.

The present results indicate that, with the exception of the 500 C samples, most of the surface area developed below 25% B.O. is essentially composed of ASA because the increase in total area was equivalent to the increase in ASA. However, at higher levels of B.O., the increase in total area far exceeds the increase in ASA, which indicates that above 25% B.O., the crystallite orientation at the exposed surface is different than at the original surface.

Deposition on VSB-32 Activated Samples

In this section we discuss the results obtained when successive layers of pyrolytic carbon were deposited, in a controlled manner, on the surface of VSB-32 activated samples, using the apparatus shown in Fig. 1. After evacuation at 1000 C to 10^{-7} Torr, a precalculated dose of ultrahigh purity methane was injected from the gas reservoir into the system. The number of methane micromoles, n , required to deposit one BET equivalent layer of pyrolytic carbon on one gram fiber was calculated in two different ways; the agreement was satisfactory. In the first method, the thickness of one layer and the density of pyrolytic carbon were taken as 0.36 nm and 2.05 g/cc, respectively. Hence, by knowing the starting surface area (SA; m^2/g) of the sample, the value of n is calculated by :

$$n = \text{SA} \times 0.36 \times \text{density} \times 1000/12 \quad (5)$$

In the second method, the number of carbon atoms, n_c , present at the external surface was calculated by :

$$n_c = \text{SA} \times 10^{18}/0.0262 \quad (6)$$

The latter denominator represents the average area occupied by one basal plane carbon atom (nm^2/atom) calculated from the geometry of the hexagonal structure of β -graphite. Since n_c can also be considered as the number of pyrolytic carbon atoms present in one BET equivalent, assuming a 1:1 carbon atom ratio, therefore:

$$n = n_c \times 10^6/N, \quad (7)$$

where N is Avogadro's number. When the sample was exposed to methane at 1000 C, the system pressure increased due to the decomposition of methane mainly into carbon and hydrogen. By monitoring the system pressure and the gas composition in the reactor, the deposition reaction was terminated when the required number of pyrolytic carbon layers was deposited, i.e., when the projected value of n was reached.

Fig. 9 represents the dependence of ASA on B.O. before deposition (lines a, b, and c) and after (line d) the deposition of one layer of pyrolytic carbon. It is evident that after the deposition of one pyrolytic carbon layer, all the samples conformed to line d regardless of the previous activation procedure used in burning off the samples before the course of deposition. Table 3 displays the values of ASA after the deposition of a second and 60 additional layers. The general trend with the four samples is essentially the same; the deposition of additional pyrolytic carbon layers on the top of the first one does not have a significant effect on changing ASA. That is, while the blockage of most active sites takes place with the deposition of the first layer, the deposition of additional layers just replicates the ASA available on the previous one.

Fig. 9 also shows two additional important features: (i) lines c and d are almost parallel and $0.11 \text{ m}^2/\text{g}$ apart, and (ii) the ASA of the samples activated to 1% B.O. is $0.12 \text{ m}^2/\text{g}$ higher than the as-received fiber ($0.029 \text{ m}^2/\text{g}$). It appears that during the first 1%

B.O., the newly generated ASA has different characteristics than that developed above 1%. The former type of sites are less stable than the latter. When pyrolytic carbon is deposited, it covers the sites that were generated below 1% and converts them to non-active sites. The deposits also cover the active sites that were developed above 1% B.O.; however, the deposits replicate the ASA developed above 1% B.O. It may be speculated that the two different types of active sites are those present as points of dislocation or imperfection at the basal planes, and those forming the edges of the crystallites. Perhaps the least stable sites are those at the edges while the more stable sites are those at points of imperfection.

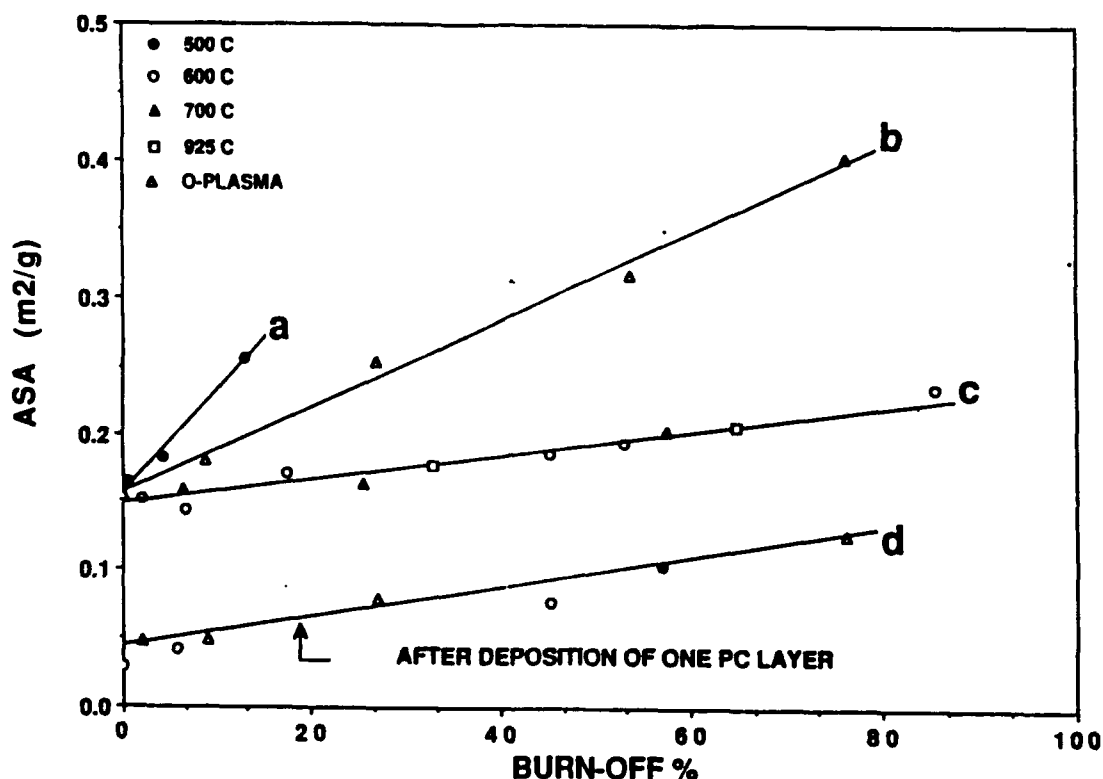


Figure 9. Dependence of ASA on Burn-Off After Deposition of One Layer of Pyrolytic Carbon.

TABLE 3. Active Surface Area (m^2/g) of Fiber Samples After Deposition of Several Pyrolytic Carbon Layers.

Number Of Pyrolytic Carbon Layers	As-Received	OP*	HTO**	OP*
		2% B.O.	6.75% B.O.	27% B.O.
0	0.029	0.156	0.143	0.243
1	0.016	0.052	0.042	0.079
2	0.018	0.034	0.027	0.072
60±5	0.038	0.048	0.036	0.070

*Oxygen Plasma Treatment

** High Temperature Oxidation Treatment At 600C

Under the experimental conditions used in this study, the deposition atmosphere could have an entire series of species ranging in size from small radicals and hydrocarbon molecules and ending with large planar "molecules" containing several carbon atoms arranged in hexagonal arrays. If the outer surface of the fiber is composed of crystallites oriented in the circumferential direction, with their basal planes running parallel to the filament axis, then the oxidation process starts and continues between adjacent crystallites to create a gap. In this case, the attack with O₂ is localized because most of the developed ASA (0.11-0.12 m²/g) is located between adjacent crystallites. During pyrolytic carbon deposition, a large aromatic molecule may fill the gap and interconnect the two adjacent crystallites with the net result of destroying or blocking the newly developed ASA. Alternatively, small radicals may chemisorb on the edges and grow until they meet with those branching from neighboring crystallites. As a result, the gap closes and the ASA is lost. As for the other type of active sites existing as defect points in the basal planes or between them, the sites may chemisorb the smaller radicals and become nonactive sites. In other words, the points of defects will end up as functional groups (e.g., -CH₃) protruding away from the basal planes. Since the probability of other radicals in the gas phase colliding with these groups is higher than colliding with the rest of the surface, an exchange reaction may propagate at these locations; the gas phase radicals are deactivated while the functional groups are converted to new active sites. Hence, the deposition of successive layers on the top of the first one keeps replicating the ASA of the localized defects.

The data and results reported in this section can be used to predict a two-dimensional model for the graphitized pitch fiber used in the study. It is recalled from Fig. 7 and Fig. 8 that between 0% and 25% B.O., the newly developed areas were only ASA, and that the ASA was always smaller than the BET area. If within this B.O. range the crystallites were oriented in the radial direction, then the total area should be active, i.e., BET = ASA. Since this is not the case, we may conclude that the orientation of crystallite below 25% B.O. is in the circumferential direction. At higher B.O., a different trend is observed; the total surface area starts increasing with B.O. at a faster rate than the ASA. It is possible that the orientation of the internal crystallites starts changing from circumferential to radial direction. If this is the case, then the deposition of the first pyrolytic carbon layer on the samples with high B.O. should show a trend different than that observed with low B.O. samples. Table 4 shows that the total area of the high B.O. samples becomes larger after deposition of the first pyrolytic carbon layer; the higher the B.O., the greater the increase in total area. A possible explanation for this, as one may propose, is that the aromatic layers of deposited pyrolytic carbon are now bonded to the edges of the radial crystallites with the net result of adding an "extension" to each crystallite. In other words, only the outer radial crystallites of the fiber are getting the extensions with the net effect of increasing the length of the pores without affecting their diameter.

TABLE 4. Total (BET) Surface Area of Fiber Samples Before and After Deposition of One Pyrolytic Carbon Layer.

Sample Pretreatment	Burn-Off	Total Surface Area (m ² /g)		% INCREASE
		Before Deposition	After Deposition	
HTO • at 500C	57.1	1.298	1.301	1.5
HTO • at 600C	45.3	0.698	0.812	16.3
HTO • at 700C	57.6	0.839	0.993	18.4
Oxygen Plasma	76.3	1.406	1.710	21.6

Based on this, the following model has been proposed for the orientation of the crystallites in a cross-section of the graphitized pitch fiber (Fig. 10). The crystallites in Region I (up to 25% B.O. or above 0.85 fiber diameter) are oriented in the circumferential direction. In Region II, the crystallites start changing direction until Region III is reached where they are essentially oriented in the radial direction. Orientation of the crystallites in the radial direction have been observed on a mesophase P55 fiber (Ref. 5). Orientation in the radial and circumference direction has also been reported (Ref. 6), depending on the spinning conditions of the fiber during processing.

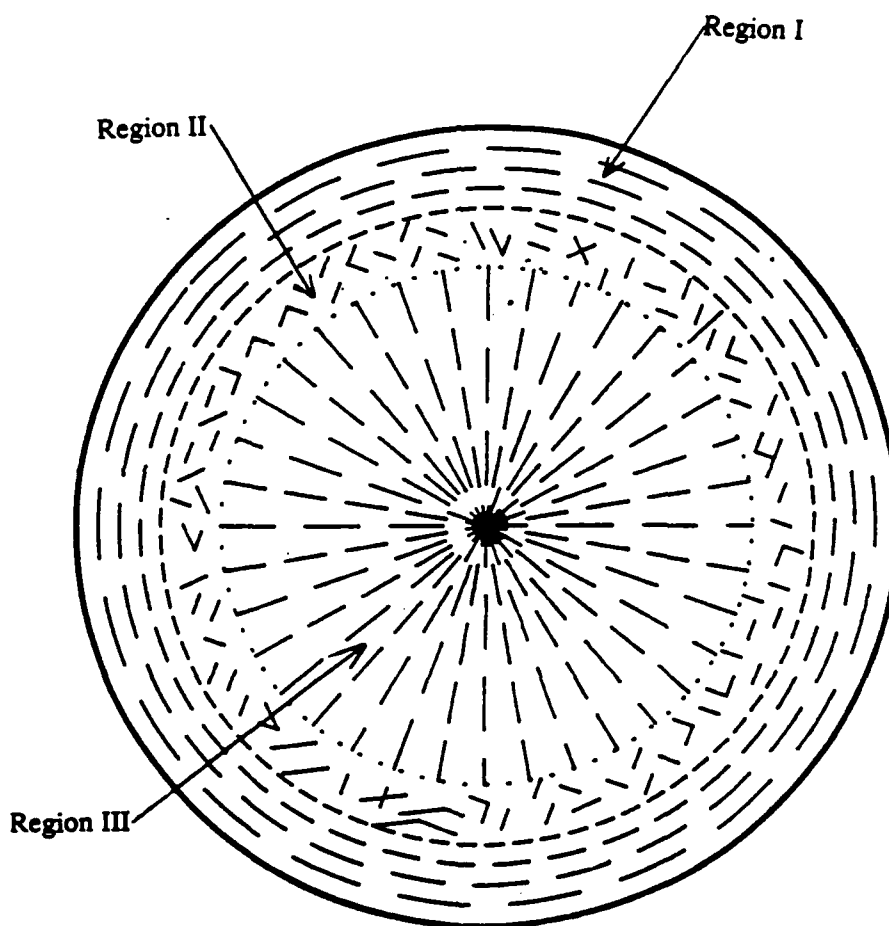


Figure 10. Proposed Model for Crystallite Orientation in a Graphitized Pitch Carbon Fiber.

Deposition on SP-1 Graphite Flakes

To investigate the effect of sample geometry on CVD rates and mechanism, a different substrate had to be used. SP-1 graphite flakes were then chosen as the appropriate candidate because they are exclusively non-porous, they have a density close to that of natural graphite (2.268 g/cc), they have very small concentrations of impurities, and they have small ASA and BET areas comparable to those of the fiber. The additional unique feature of the flakes is the way the active sites are located with respect to the non-active ones (at basal planes). The top and bottom of each flake are essentially composed of basal planes while the sides are composed mainly of active centers (i.e., edge carbon atoms). If, under one set of experimental conditions, the CVD reaction is taking place only at the active sites, then at some point in time the flakes should be bonded together through their sides and the surface morphology at the top and bottom of the flakes should remain unchanged. This could easily be observed by examining the samples using a scanning electron microscope (SEM). On the other hand, if the deposition is taking place at the sides as well as on the top and bottom of the flakes, i.e., the deposition occurs on the entire surface of the flakes, then both surfaces (active and non-active) would be contributing to the deposition mechanism, and as a result, the morphology of the entire flake would change.

The SP-1 used in the present section was first activated at 650 C in air inside a muffle furnace until the flakes reached the 12.4% level of B.O. The activated sample had a starting ASA value of 0.24 m²/g and a starting total BET area of 3.81 m²/g. Following activation, the samples were evacuated at 1000 C, as was the case with the VSB-32 fiber, and a systematic deposition of pyrolytic carbon layers was performed. First one pyrolytic carbon layer, equivalent to one ASA, was chemically deposited on the samples at 1000 C, then the ASA was determined using oxygen chemisorption at 300 C. Next, another 1.7 ASA equivalent layers were deposited on the sample and once again the ASA measurement was performed. This cycle was repeated several times until 542 layers of ASA equivalents were deposited. The results of this series of tests are summarized in Table 5. It is evident that after two ASA equivalents were deposited on the sample, the ASA became essentially constant. The deposition of additional layers showed negligible changes in the ASA value. It can be stated that the final ASA of this activated sample can be averaged to a constant value of 0.155 ± 0.015 m²/g after the deposition of two or more CVD layers.

TABLE 5. Variation of ASA With the Number of CVD Layers Deposited on SP-1 Graphite Activated to 12.4% B.O.

Number Of CVD Layers	ASA(m ² /g)
0	0.24
1	0.21
2.7	0.14
6.3	0.15
51.4	0.17
113	0.16
205	0.14
297	0.14
417	0.15
542	0.14

Occasionally after terminating some of the ASA experiments and before adding the subsequent CVD layers, the total (BET) was measured. The results, summarized in Table 6, indicate that the total (BET) area is not appreciably changing with the amount of deposit. The table also shows that the ratio ASA/total area remained constant. That is, in spite of the drop in both ASA and BET area after the deposition, the population of active centers with respect to the entire surface remains essentially unchanged.

TABLE 6. ASA and Total BET Areas of SP-1 Graphite Sample Activated to 12.4% B.O.

Number Of CVD Layers	ASA(m ² /g)	BET Area (m ² /g)	ASA/ BET * 100
0	0.24	3.81	6.3
6.3	0.15	N/A	N/A
113	0.15	N/A	N/A
297	0.14	2.57	5.5
417	0.15	2.23	6.7
542	0.14	2.36	5.9

N/A: Not Available

The edges of the flakes are essentially composed of active sites whose carbon atoms have valence electrons which could form chemical bonds with other species present in the deposition medium. When methane cracks, it yields several radicals, either atomic or molecular, and large polymeric groups. It is therefore feasible for some of these species to bond with one or more edge carbon atoms. Consequently, both ASA and total BET area decrease. Eventually, after three layers of deposition, some of the edge atoms are either bonded to each other through the pyrolytic carbon radicals or they are completely blocked. Additional deposition would then generate ASA at the same rate of disappearance of the old ASA. In other words, after the third CVD layer, the ASA keeps replicating itself and most of the available active sites are those present on the deposit.

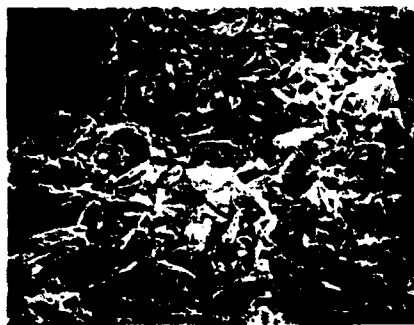
The decrease in ASA, from 0.24 to 0.15 m²/g, cannot account for the decrease in total BET area, which was well above 1.0 m²/g. Therefore, during the deposition reaction, some flakes were agglomerating to form larger particles. Scanning electron micrographs of SP-1 samples before and after deposition of pyrolytic carbon at 1000 C are displayed in Fig. 11. The as-received sample, plate (a), is composed of flakes having different particle sizes with a wide range of size distribution. At a higher magnification, plate (b), the graphitic surface is observed, the side of the flakes (which is composed essentially of active sites) looks rather sharp, and smaller flakes override the larger ones. This means that at the commencement of deposition, most of the carbon is deposited on active sites. At this low level of CVD, the active sites of the larger flakes are probably connected to those of the smaller ones via intermediate planner aromatic molecules. After 7.1% deposit, plate (d), the trend continues with more accumulation on the sides and a noticeable deposition on the graphitic surface (top and bottom of the flakes). After the deposition of 16.1%, the flakes that were originally long and thin become completely covered with smaller particles as well

as pyrolytic carbon, plate (e). However, the larger flakes are covered essentially with only pyrolytic carbon deposits, plate (f). In the latter case, the build up and thickness of deposits at the edge of the particles is greater than that observed at other locations. This trend continues at higher levels of deposition with further agglomeration of the particles. For example, at the 52.5% level, smaller particles were generally not seen except in few cases as shown in plate (g) where the flakes, in this particular case, are joined together side by side. In some instances, however, the particles were sitting on the top of each other as shown in plate (h). It is noted that the deposits on the sides have a fine grain and appears smoother than those coarse deposits formed on the top of the flakes. This means that the nature of the surface, on which the deposition takes place, plays a major role in affecting the surface morphology of the end product. The basal plane areas tend to yield coarse deposits but the active sites yield a smooth surface.

Deposition in the Flow Reactor

Effect of Temperature and Substrate on Deposition Rates

Typical thermograms obtained with the TGA on the VSB-32 fiber are shown in Fig. 12. It is seen that sample temperature has quite a dramatic effect on deposition rates and carbon yields. For example, after 15 h exposure, the yields, based on the starting weight of the fiber, were 19% at 1005 C and 125% at 1080 C. Dependence of rates on sample temperature (Arrhenius plots) are illustrated in Fig. 13 for the VSB-32 fiber as well as other selected carbons. These plots, in the temperature range of 1000 to 1100 C, are also linear; their slopes have been used to compute the corresponding values of activation energy (E_a). The values of E_a are related to the starting BET surface area, as shown in Fig. 14. For the carbon having the smallest BET area, the activation energy is 98 kcal/mole. As the surface area increases, the activation energy drops and finally attains a constant value of about 55 kcal/mole for the samples having BET areas of 60 m²/g and higher. Since the average energy required to break a C-H bond in methane molecules is 104 kcal/mole (Ref. 7), we may then conclude that the surface of the substrate catalyzes the deposition reaction, and thus, enhances the rate at which the hydrocarbon bonds are broken. In other words, in the absence of a substrate, methane molecules may crack in the gas phase with minor deposition of pyrolytic carbon only on reactor walls. The activation energy in this case would be in the vicinity of 104 kcal/mole. When a carbonaceous substrate is placed inside the reactor under similar experimental conditions, methane molecules collide more effectively with the carbon surface than with each other. That is, the probability of breaking the C-H bonds at the surface is higher than in the gas phase. A larger substrate surface area yields a higher probability of collision, a faster CVD rate, and with it, a lower activation energy for the deposition reaction. With a faster CVD rate, the fiber bundles or carbon particles are bonded together faster, and the starting surface area is also decreased faster. This means that the starting surface of the substrate is contributing to the CVD reaction in three ways: enhancing the rate, lowering the activation energy, and accelerating the rate of decreasing surface area. The first condition is supported by the data displayed in Fig. 15. As the surface area increases, the deposition rate (R_1) increases and



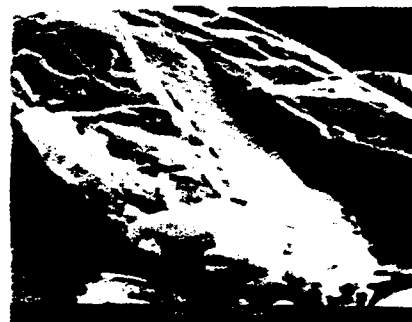
(a) As - Received SP - 1



(b) As - Received, higher magnification



(c) After deposition of 2.4% pyrolytic carbon



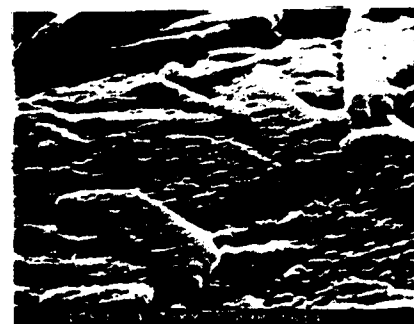
(d) After deposition of 7.1% pyrolytic carbon



(e) After deposition of 16.1%



(f) After deposition of 16.0%



(g) After deposition of 52.5%



(h) After deposition of 52.5%

Figure 11. Scanning Electron Micrographs of SP-1 Graphite Before and After Deposition of Pyrolytic Carbon

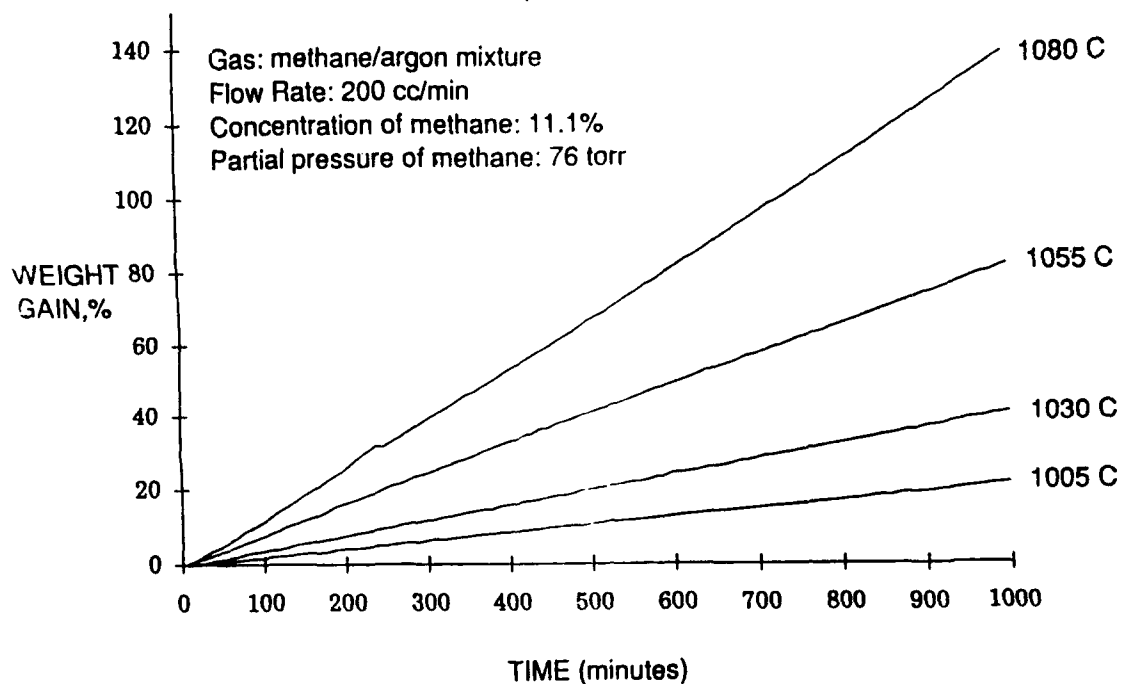


Figure 12. Typical Thermograms for Methane Cracking Over VSB-32 Fiber (Flow System).

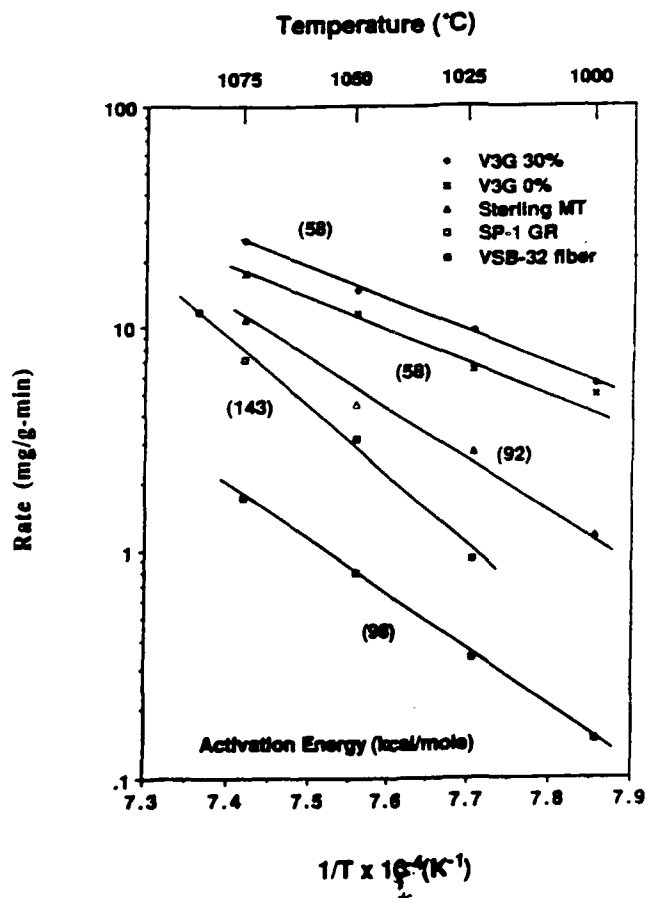


Figure 13. Dependence of CVD Rates on Reaction Temperature.

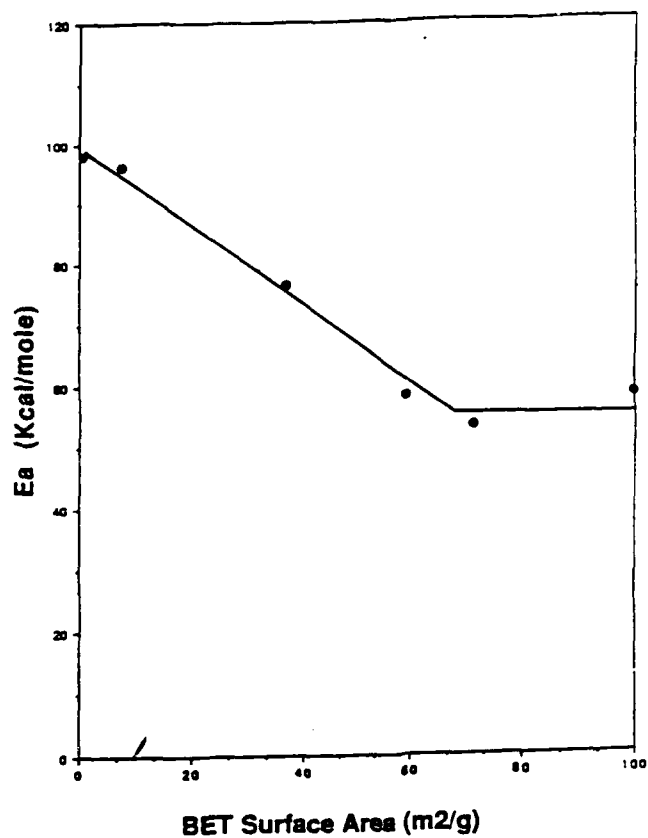


Figure 14. Variation of Activation Energy with Starting Surface Area.

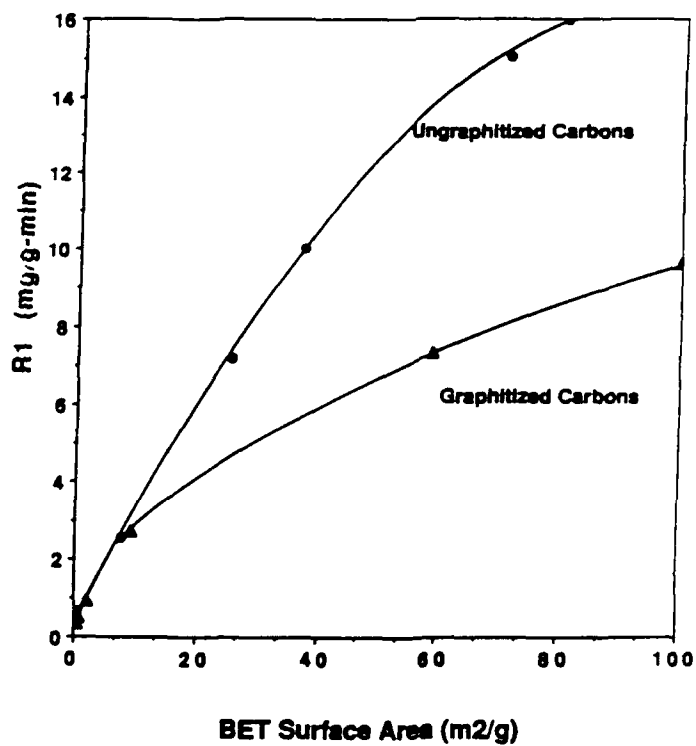


Figure 15. Effect of Starting Surface Area on Deposition Rate (mg/g-min).

the rates on ungraphitized carbons are higher than those on the graphitized substrates. The third condition is supported by the data shown in Fig. 15. The rates (R2), expressed per unit surface area of the material, are dropping with increasing surface area of the carbons. This means that the efficiency of using the starting surface area is at its best with the carbon having the lowest surface area. It is evident, therefore, that with each material there is always a compromise between the rate of accelerating the reaction and the rate of losing the surface area or slowing down the reaction. Apparently, with carbons having BET areas smaller than $55 \text{ m}^2/\text{g}$, the net result is an acceleration effect. However, with carbons having $55 \text{ m}^2/\text{g}$ or higher, the rate of accelerating the reaction is offset by the rate of surface area disappearance.

It is also seen in Fig. 15 that, for a given value of surface area, the CVD rate on an ungraphitized carbon is higher than on a graphitized one. Graphitized carbon blacks are generally composed of agglomerates of smaller particles, while ungraphitized carbons are composed essentially of small loose particles. It appears then that once the deposition reaction begins on graphitized carbons, a large portion of the entrances to internal particles inside the agglomerates is partially or completely blocked with the carbon deposited from the gas phase. This, in turn, would decrease the fraction of the starting area available for collision with methane molecules, and would ultimately lower the observed CVD rate. The same scenario can also be extended to explain the data displayed in Fig. 16 which clearly indicate that the surface of the ungraphitized carbons is used more effectively in the deposition reaction than the surface of graphitized carbons.

Pyrolytic Carbon Deposition on Carbon Fibers

Since the main objective of this work is to understand the mechanism of CVD on carbon fibers, special emphasis was given to these materials. In this section, the results obtained on two carbon fibers and one fabric are discussed. The T-300 fiber is a carbonized polyacrylonitrile fiber, the VSB-32 is a graphitized pitch fiber, and the WCA is a rayon fabric that had been heat treated to a temperature in the range of 2200-2500 C. Fig. 17 illustrates the thermograms obtained at 1025 C when the three materials, as well as SP-1 graphite, were exposed to a mixture of 10% methane in argon. For the four samples, the increase in sample weight is linearly related to exposure time. The deposition rate ($\text{mg/g}\cdot\text{min}$), calculated as the slope of the line and based on the starting weight of substrate, is the highest for SP-1 graphite and T-300 fiber (superimposed lines), and the lowest for the graphitized pitch fiber. Since the CVD is a heterogeneous reaction, the linearity of the lines suggest that, as long as the reaction is progressing, the deposits keep replicating their characteristics. It is seen from Table 7 that SP-1 has the smallest interlayer spacing and the largest crystallite size. This means that of the four samples, SP-1 is the most graphitic carbon; yet its deposition rate is equal to that of the carbonized fiber (T-300) and higher than the other two carbons.

From the values of ASA and TSA, two additional deposition rates were estimated: RTSA, the rate normalized to the starting total surface area ($\text{mg}/\text{m}^2 \text{ TSA} \cdot \text{min}$), and RASA, the rate normalized to the starting active surface area ($\text{mg}/\text{m}^2 \text{ ASA} \cdot \text{min}$). These rates, which are listed in Table 8, show three main features. First, with the most graphitic material, RASA is the highest but RTSA is the lowest. This means that if the deposition is occurring only on the active sites, the efficiency is at its best. On the other hand, if it is occurring on the total area (mainly basal planes in this case) the rate is the lowest. In fact, under the present conditions, it is hard to predict whether the deposition is preferentially taking place on the active centers or on the entire surface of the substrate. Second, there is no definite correlation between RTSA and TSA or RASA and ASA. That is, neither the starting value of TSA nor that of ASA can normalize the rates. Third, the only feasible

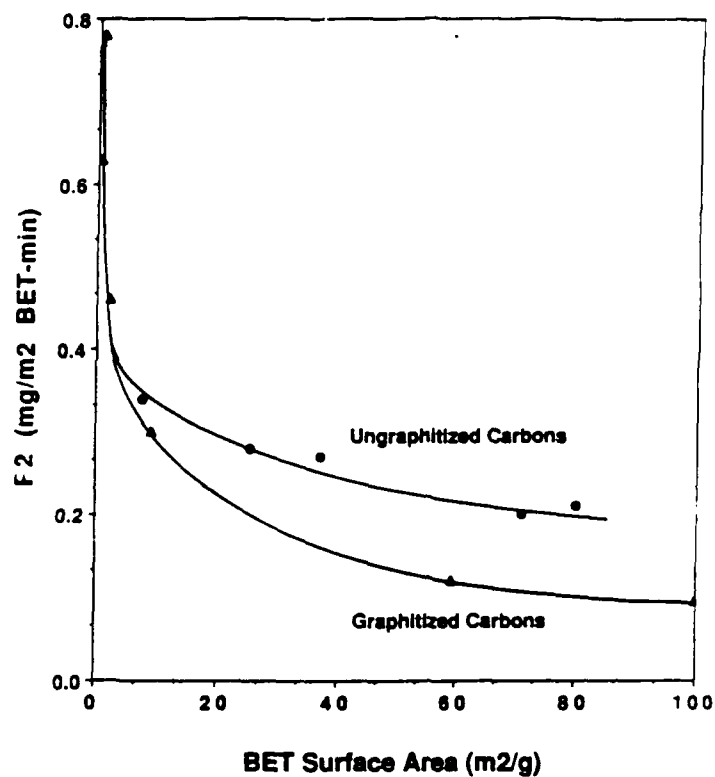


Figure 16. Effect of Starting Surface Area on Deposition Rate (mg/m²-min).

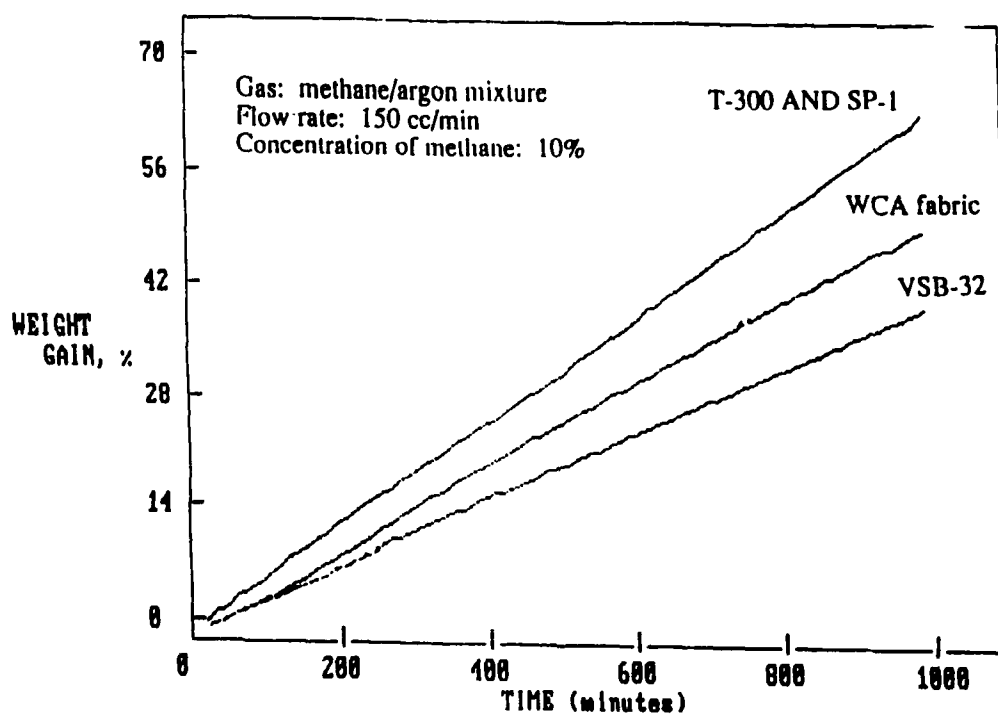


Figure 17. Raw Data for the Deposition of Pyrolytic Carbon on Carbon Substrates at 1025 C.

relation is the dependence of the original rate (mg/g · min) on TSA and this has been discussed in the previous section (Fig. 15).

TABLE 7. X-ray Parameters of Carbon Fibers and SP-1

Material	Interlayer spacing (nm)	Crystallite height Lc (nm)	Crystallite width La (nm)	X-ray** density (g/cc)
T-300	N/A*	N/A*	N/A*	N/A*
WCA	0.3455	3.5	3.0	2.202
VSB-32	0.3435	9.0	3.0	2.214
SP-1 Graphite	0.3354	∞	∞	2.268

*Not Applicable: No diffraction peaks were obtained. This fiber seems to be non-crystalline.

**Calculated as $2.268 \times 0.3354 / d_{002}$

TABLE 8. Active Surface Area (ASA and Deposition Rates of Selected Carbons.

	ASA (m ² /g)	TSA (m ² /g)	Deposition Rate		
			(mg/g/min)	(mg/m ² TSA·min)	(mg/m ² ASA·min)
T-300	0.075	0.56	0.644	1.15	8.59
WCA	0.068	0.66	0.500	0.76	7.35
VSB-32	0.029	0.54	0.340	0.63	11.72
SP-1	0.049	2.00	0.651	0.33	13.29

Effect of Gas Composition

For the VSB-32 fiber, the dependence of deposition rate on gas composition between 1025 and 1075 C was studied. Fig. 18 displays the effect of gas composition on CVD rates. Increasing the hydrocarbon concentration in the mixture enhances the rates because the number of hydrocarbon molecules, and hence the concentration of reactive species per unit reaction volume, is raised. The slope of the lines was used to compute the order of the reaction which was close to unity (0.91). Therefore, for the deposition of pyrolytic carbon on the surface of VSB-32 fiber, the reaction is first order with respect to methane concentration. This suggests that the deposition reaction starts by the decomposition of methane in the gas phase.

In Fig. 19, the same data are plotted in the form of an Arrhenius plot. It is seen that when the concentration of methane in the flowing gas increases, the activation energy also increases. This may only be true in the case of VSB-32 fiber and may not be valid with

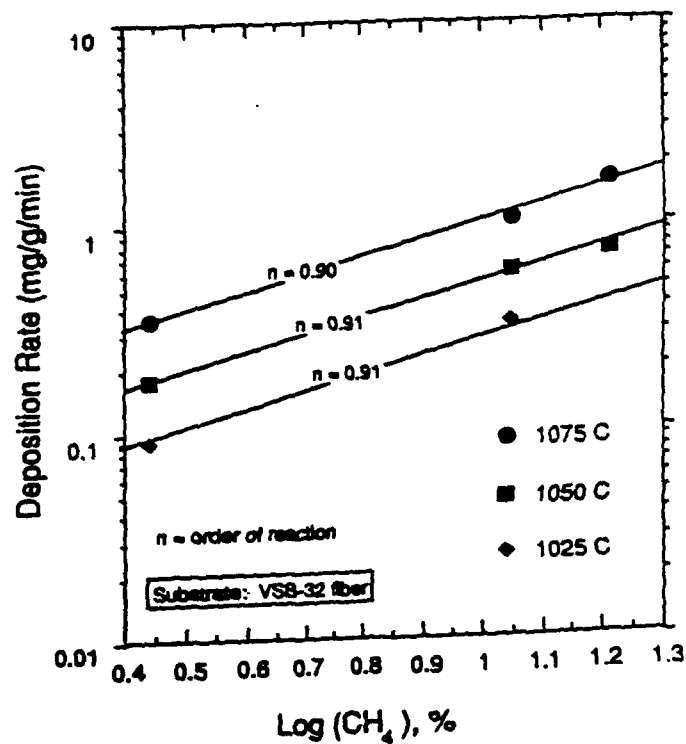


Figure 18. Dependence of CVD Rates on Methane Concentration.
Temperature (C)

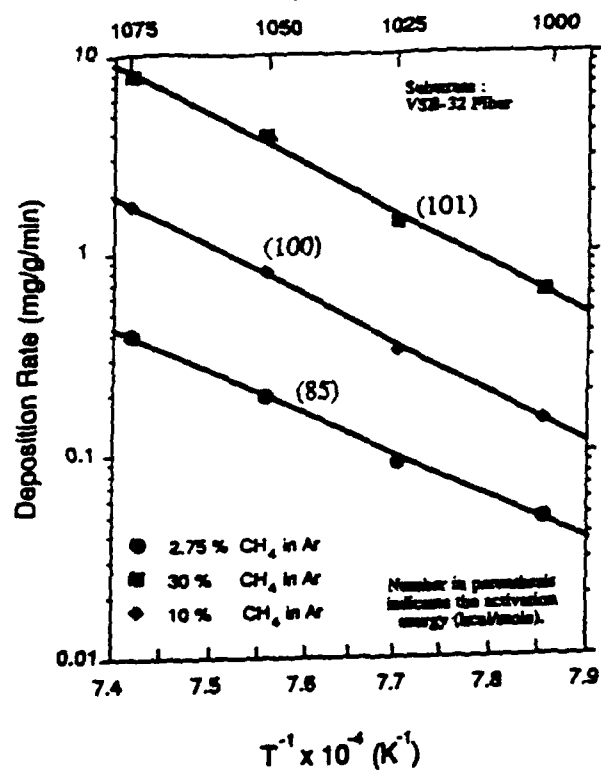


Figure 19. Dependence of Deposition Rate on Temperature (Arrhenius Plots) and Gas Composition.

other carbonaceous substrates. The increase in activation energy with gas composition may be attributed to the by-products of methane decomposition. As mentioned earlier, the mechanism of deposition on this fiber is essentially controlled by dissociation of methane in the gas phase to yield hydrogen as the main product. It is possible that H_2 acts as an inhibitor to the deposition reaction. The exact mechanism of inhibition is not fully understood; however, the following speculations may be given. Hydrogen could be chemisorbed on carbon active sites, it could inhibit the growth of smaller species to form large aromatic molecules in the gas phase, or it may accelerate the opposite reaction, i.e. recombination of products to yield reactants. This subject will be further investigated during the next few months.

Effect of Flow Rate

The effect of gas flow rate above the samples on the rate of pyrolytic carbon deposition was studied at 1025 C on two different substrates; VSB-32 fiber (surface area = $0.54 \text{ m}^2/\text{g}$) and V3G carbon black (surface area = $59.2 \text{ m}^2/\text{g}$). In both cases, the concentration of methane in the flowing gas was held constant at about 10%, and the flow rate of the mixture during deposition was varied between 10 and 300 cc/min. The results, displayed in Fig. 20, show that by increasing the gas flow rate, the deposition rate can either decrease, as is the case with the VSB-32 fiber, or increase as is the case with V3G. This suggests that there are at least two different mechanisms for the CVD on carbon substrates, depending on the type of carbon used. With a small surface area material, the reaction starts in the gas phase and ends on the substrate surface. Increasing the flow rate inside the reactor will shorten the residence time of methane, and as a result, the flowing gas will not attain a high temperature as it would normally reach with a small flow rate.

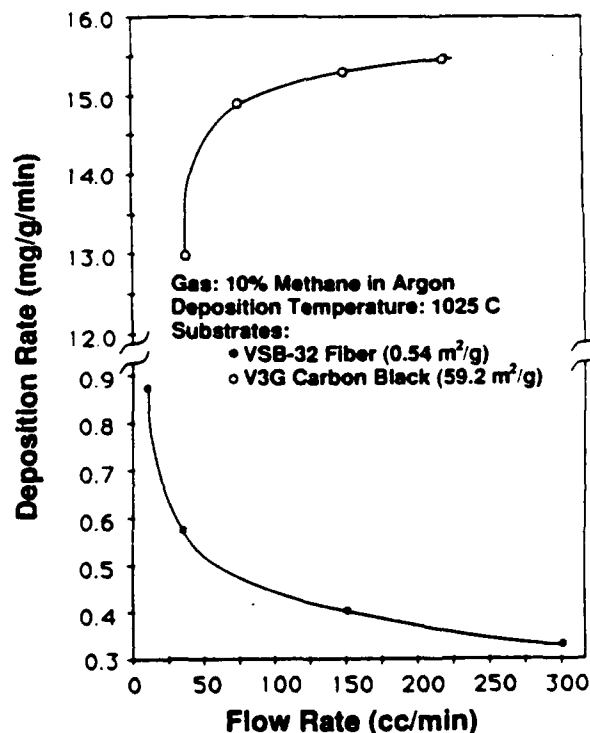


Figure 20. Influence of Gas Flow Rate on Pyrolytic Carbon Deposition Rates.

Therefore, the process of decomposing methane in the gas phase is slowed down and the deposition rate on the VSB-32 fiber decreases. That is, the rate-determining step with a small surface area carbonaceous sample is the decomposition of hydrocarbon molecules in the gas phase.

On the other hand, with a large surface area material, the rate determining step is the direct collision between methane molecules, or one of their intermediate species, and the substrate. Hence, when the flow rate inside the reactor increases, the number of collisions between the reactive species and the surface of substrate is higher, and the deposition rate increases.

Properties of Deposits

Deposits on VSB-32 Fibers

To better understand the mechanism of deposition on carbon substrates, different samples were prepared under a wide range of experimental conditions and the composites produced were then characterized. With the VSB-32 fiber, several samples were prepared in both static and flow reactors.

In the static reactor, fresh as-received fiber samples were evacuated at 1000 C to better than 10^{-7} Torr, then subjected to a dose of ultrahigh purity methane at a starting pressure in the range of 1 to 200 Torr. At all pressures, the samples were kept for 15 h in contact with the unreacted methane and product gases. In the flow reactor, the as-received fiber was evacuated, flushed with nitrogen, then heated for two hours at 1273 K in nitrogen flowing at 200 cc/min. At the end of this period, a mixture of 12% methane in argon was flowed to replace nitrogen at the same rate. The reaction was continued for different lengths of time to achieve different levels of deposition. After terminating each run, the percent of deposit on the fiber samples was estimated by weight difference.

Fig. 21 illustrates how the surface area of the samples changes with the amount of carbon deposited under different conditions. In the static reactor, as the starting pressure of methane increases above 2 Torr, the amount of deposit in 15 h increases and the surface area is enhanced. For these samples, the surface areas were generally higher than the starting value of the as-received fiber. By contrast, the surface areas of all samples prepared in the flow reactor were lower. This means that at 1273 K, the static reactor deposits more porous pyrolytic carbon than the flow reactor. To further support this finding, a flow reactor sample with 33% deposit (surface area = $0.56 \text{ m}^2/\text{g}$) was placed inside the static reactor and exposed to a 100 Torr methane dose for 15 h at 1273 K. As a result, the sample gained an additional 3.5% deposit, i.e., the total weight gain became 36.5%, and the surface area increased to $0.82 \text{ m}^2/\text{g}$ (point A in Fig. 1). This means that whether the CVD reaction in the static reactor is carried out on a clean fiber surface or on the surface of a fiber previously covered with pyrolytic carbon, the surface of the deposits in both cases is more porous than the original substrate.

The data displayed in Fig. 21 have other important features. The bottom line in the figure represents the (theoretical) geometric surface area based on the diameter of the fiber and its density assuming that the deposition has not progressed to the point of joining the filaments. For the as-received fiber, the density and average diameter are 2.037 g/cc and 10.67 micron, respectively. These values yield a geometric area of $0.184 \text{ m}^2/\text{g}$ which is equivalent to approximately 1/3 of the total BET area. Further, for a fiber with a given amount of pyrolytic carbon deposit, the diameter is primarily dependent on the actual density of the deposit. If one assumes the two extreme cases with pyrolytic carbon

densities of 1.2 and 2.2 g/cc (Ref. 8,9), the calculated geometric areas of a fiber sample with 33% deposit would be 0.229 and 0.210 m²/g, respectively. That is, if the deposits are exclusively nonporous, the increase in geometric area at the 33% CVD level is about 15%. However, as the theoretical calculations show, the effect of density on the geometric area is generally not very pronounced.

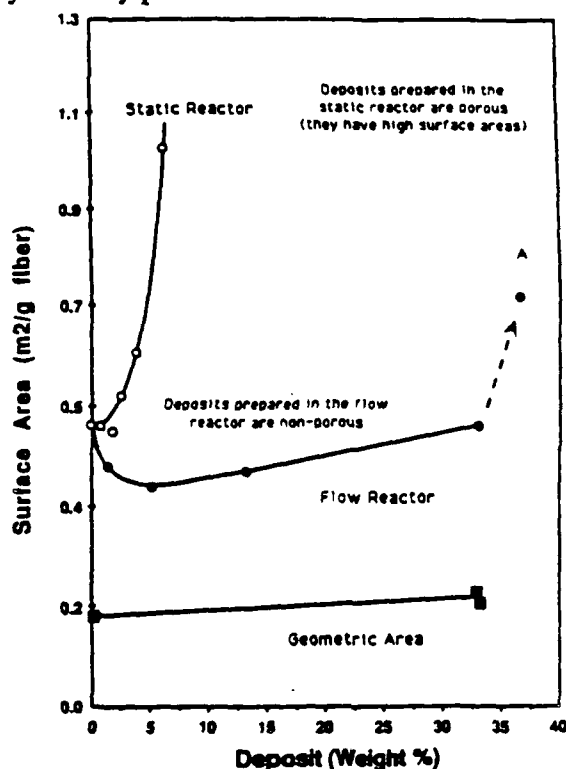


Figure 21. Surface Area of Deposits Prepared in Flow and Static Reactor.

The surface areas of the flow reactor samples show two distinct regions one between 0 and 5% deposit where the surface area decreases while the CVD level increases, and the other between 5 and 33% deposit where the surface area increases linearly with the amount deposited. In the first region, the deposit is presumably covering a portion of the original fiber roughness while the diameter is simultaneously increasing. The rate of the former process exceeds that of the second with a net decrease in surface area. Above the 5% CVD level, most of the roughness has been coated with a smoother deposit, and the increase in area is due solely to an increase in fiber diameter. The fact that the slope of the linear region in this case is higher than the corresponding slope obtained for the computed geometric area (bottom line in Fig. 21), can be attributed to development of roughness. In other words, it is possible that at low levels of CVD, the deposits are smooth, but as the CVD level increases, the deposits become somewhat rough.

In the case of the static reactor, there is no appreciable change in surface area up to 2% deposit. This means that the deposits are either replicating the roughness originally present with the fiber, or that the rate of removing the original roughness due to pyrolytic carbon deposition is equal to the rate of introducing a new porosity in the deposit. As more pyrolytic carbon is deposited above the 2% level, the amount of porosity is high and the surface area increases at a fast rate. This finding, along with the one discussed in the

previous sections, suggests that the porosity of pyrolytic carbon at a constant deposition temperature may depend not only on the type of reactor used but also on the amount of deposit.

Scanning electron micrographs for two fiber samples having a similar weight gain of about 33% are displayed in Fig. 22. As plates (a) and (b) show, up to this level of weight gain the deposits are uniform around the fiber filaments, and the agglomeration process has not yet begun since gaps between the fiber filaments can still be seen. It appears that above this level of CVD, the mechanism begins changing from simple fiber coating to a combination of fiber coating and infiltration inside the gaps present between the filaments. At higher magnification, plates (c) and (d), additional features of the deposits can be seen. With the flow reactor, the deposits appear dense with a smooth surface, but those prepared in the static reactor are rough and porous. This means that at 1273 K, the CVD mechanism is not the same in both reactors.

It is known that the nature and properties of pyrolytic carbon deposits are extremely sensitive to the experimental conditions under which the deposition takes place (Ref. 9-11). At low temperatures (at least 900-1100 C) and low hydrocarbon pressures (below 10 Torr), a dense deposit, with laminar structure and clear characteristic growth features, is produced (Ref. 9). That is, a high density layered pyrolytic carbon is deposited. As the hydrocarbon pressure increases, the density decreases, the growth features start disappearing, and a laminar aromatic type of pyrolytic carbon (rich in its hydrogen content) is produced (Ref. 9). In either case, the large planar molecules are first formed in the gas phase then later deposited on the substrate (Ref. 10). In the present study, as the starting pressure in the static reactor increases, the deposits become more porous. With increasing methane pressure in the reactor, the pressure of product gases (mainly hydrogen) is also raised, and the rate of other side reactions is higher. For example, the presence of high concentrations of hydrogen in the medium can either enhance the rate of C/H₂ reaction or retard the formation and growth of the laminar aromatic molecules. In the former case, porosity would develop due to the gasification of a fraction of the pyrolytic carbon just deposited, while in the latter case, smaller aromatic molecules are deposited randomly on the surface to form a porous carbon. The presence of hydrogen in the deposition medium is known to have a dramatic effect not only on lowering the CVD rates (Ref. 12) but also on changing the properties of the deposit (Ref. 13).

Deposits on V3G Carbon Black

Now we discuss the surface area of the samples prepared at 1025 C by deposition of pyrolytic carbon on a V3G substrate. In these experiments, a 10% methane in argon gas mixture was flowed above the sample at 150 cc/min. Dependence of surface area on the amount of deposit is displayed in Fig. 23. As the amount of deposit increases to 15% weight gain, the surface area increases and attains a maximum. This means that with the first few percent of deposit, either the particles are interconnected and some porosity is developed, or the deposits start by forming small particles on the top of the large substrate particles. As the deposition continues above 15%, the pores are blocked, small particles grow to larger ones, and the structure changes smoothly from loosely bound particles to agglomerates to larger "chunks." With this change, the surface area keeps decreasing with the amount of deposit. The fact that above 100% weight gain, the surface area starts leveling off indicates that at this level, the CVD reaction is taking place on almost a flat composite surface below which the original particles of the substrate are embedded.

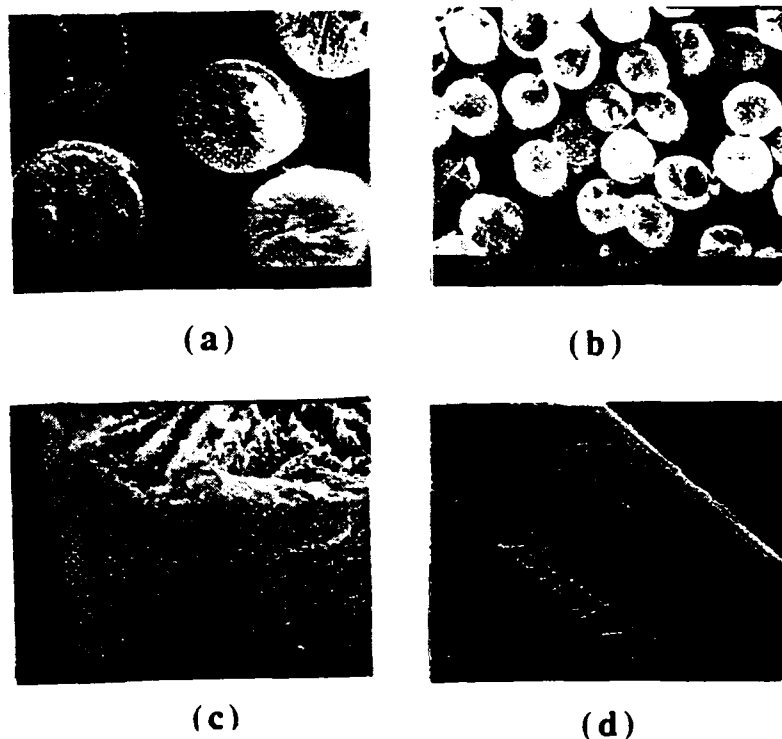


Figure 22. Scanning Electron Micrographs of VSB-32 Fiber Coated at 1273 K with 33% Pyrolytic Carbon: (a) and (c); Static Reactor, (b) and (d); Flow Reactor.

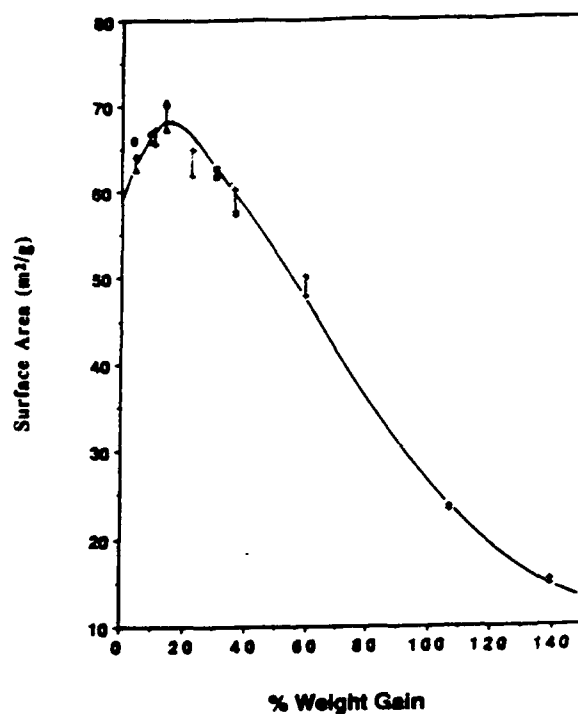


Figure 23. Surface Area of Carbon-Carbon Composites Prepared at 1025 C (Starting Substrate: V3G).

Mechanisms of Deposition

From the data generated in static and flow reactors, the following mechanisms may be proposed. In the static reactor (Fig. 24), hydrogen stays in deposition medium, the gas may react with other intermediate gaseous species, or it may gasify the carbon deposits. In the former case, the intermediate species will not have enough chance to grow in size. As a result, small grains will deposit randomly on the substrate. Further, the reaction between hydrogen and carbons could be significant at 1000 C; thus the carbon deposit could be gasifying during the course of deposition. Obviously the net result will depend on how fast the carbon is laid down and how fast it is gasified. Apparently, under the present experimental conditions, the rate of gasification is not as high as that of deposition and the overall net observed effect is a weight gain. With either explanation, the end product is somewhat porous.

In the flow reactor (Fig. 25), hydrogen does not exist at high levels because it is instantaneously removed from the medium. Therefore, the intermediate species will have a good chance to grow in size and large planar molecules will deposit on the surface. Since hydrogen is not present in the medium, the carbon deposits will not gasify and their structure remains intact. In other words, the large planar molecules, which are formed in the gas phase, are directly deposited on the substrate surface without any further disturbance. This will yield a somewhat nonporous deposit.

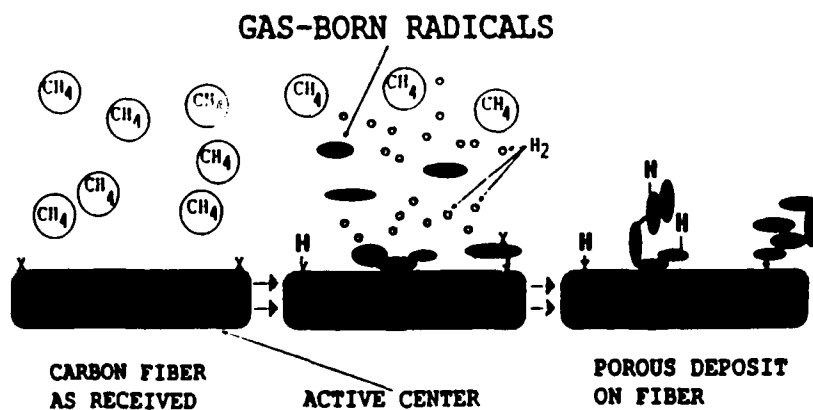


Figure 24. Proposed Mechanism of CVD in Static Reactor.

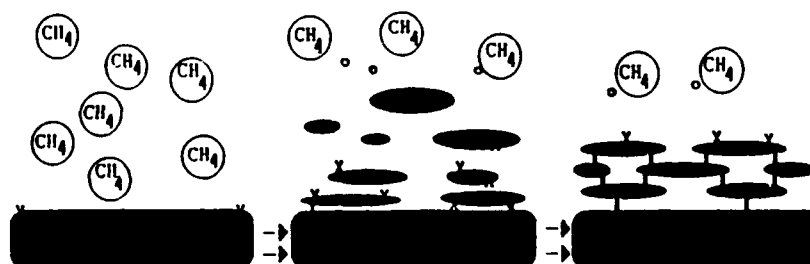


Figure 25. Proposed Mechanism of CVD in Flow Reactor.

CONCLUSIONS AND RECOMMENDATIONS

1. Cracking of methane over pitch carbon fiber surface is sensitive to the type of reactor used. Under similar experimental conditions (sample temperature and starting concentration of methane), the CVD rate and yield in a flow reactor are substantially higher than in a static reactor. For example, at 1000 C and methane partial pressure of 76 Torr, the flow system enhances the rate of CVD by a factor of 5. This may be attributed, in part, to the removal of some products (H_2) from the reaction medium and elimination of C/ H_2 gasification reaction.
2. For pyrolytic carbon deposition on pitch fiber, the activation energy between 1000 and 1100 C is 85-101 kcal/mole depending on methane concentration.
3. The presence of hydrogen retards the rate of reaction, changes the mechanism of deposition, and affects the properties of the end product.
4. In the flow reactor, the reaction is almost first order with respect to the partial pressure of methane.
5. Between 1000 and 1075 C, the deposition of pyrolytic carbon over the surface of non-porous carbons under flow conditions is not only sensitive to the experimental parameters of the reaction but also to the nature of the carbon substrate under consideration. If the carbon substrate has a small surface area, the rate controlling step is the dissociation of methane in the gas phase, i.e., the cleavage of C-H bonds. On the other hand, if the carbon has a large surface area of 60 m^2/g or above, the dissociation and deposition occur directly on the surface of the substrate.
6. A model has been proposed for the orientation of the crystallites in a cross-section of the graphitized pitch fiber (Fig. 10). The outer crystallites, i.e., in Region I (up to 25% B.O.

or above 0.85 fiber diameter) are oriented in the circumferential direction. In Region II, the crystallites start changing direction until Region III is reached where they are essentially oriented in the radial direction.

7. To use the CVD process for preparing C-C composites, the following recommendation may be given. It is recalled from previous sections that the deposits on the pitch carbon fiber under static conditions are more porous than under flow conditions. In other words, the deposits of the static reactor have more surface heterogeneity than those of the flow reactor. A heterogeneous surface is more desirable for improving the interaction between a matrix and a fiber surface during the preparation of composites. Since the static reactor deposits are rich in hydrogen, formation of more functional groups between the matrix and the deposits will occur and would ultimately lead to better mechanical properties of the composites. In addition, the improvement in mechanical properties will take place as a result of the enhanced surface area available for direct contact with the matrix, as a result of the introduction of pores which improve the mechanical interlock with the matrix, and as a result of higher population of hydrogen functional groups, which enhances the number of chemical bonds. On the other hand, the deposits formed in the flow reactor (i.e., with a low surface area and insignificant porosity) have more desirable properties for the surface of the final end product. Perhaps the most reasonable approach for preparing an acceptable composite, via pyrolytic carbon deposition on an as-received fiber or fabric, is to use a cyclic combination of both systems, i.e., to deposit successive pyrolytic carbon layers under alternating static and flow conditions. The first layer should be deposited under static conditions so that its surface can be used to improve the adhesion with the second layer deposited under flow conditions. The two successive steps are then continued in this manner until the required composite is made. It is recommended that the final cycle has to be performed under flow conditions so that the last layer can block the residual porosity developed in the previous cycles and deactivate the final external surface of the composite.

REFERENCES

1. Brunauer, S., Emmett, P. H., and Teller, E., "Adsorption of Gases in Multimolecular Layers." Journal of the American Chemical Society, Vol. 60, p. 309, 1938.
2. Ismail, I. M. K. and Hoffman, W.P., "Cross-sectional Area of Krypton on Graphitized Carbons at 77K." 19th Biennial Conference on Carbon, The Pennsylvania State University, p. 18, June 1989.
3. Ismail, I. M. K., Improved Carbon-Carbon Fiber Matrix Adhesion (Surface Properties of Fibers), AFRPL TR-85-095, UDRI, Edwards AFB, CA, April 1986.
4. Ismail, I. M. K., "Structure and Active Surface Area of Carbon Fibers." Carbon, Vol. 25, p.653, 1987.
5. White, J. L., Ng., C. B., Buechler, M., and Watts, E. J., "Microstructure of Mesophase Carbon Fiber." 15th Biennial Conference on Carbon, University of Pennsylvania, p. 310, June 1981.
6. Hamada, T., Sajiki, Y., Furuyama, M., and Tomioka, T., "Structural Development of Pitch Based Carbon Fibers by Heat Treatment." 18th Biennial Conference on Carbon, The Worcester Polytechnic Institute, p. 227, July 1987.

7. CRC Handbook of Chemistry and Physics, 58th Edition, p. 231, 1977-1978.
8. Raveh, A., Eldan, M., Inspektor, A., and Avini, R., "Structure of the Solid Pyrolysis Products From Propylene in a Low-Pressure Inductive R.F. Plasma." Carbon, Vol. 23, p. 179, 1985.
9. Kotlensky, W. V., "Deposition of Pyrolytic Carbon in Porous Solids." Chemistry and Physics of Carbon Vol. 9, p. 173, 1973.
10. Bokros, J. C., "Deposition, Structure, and Properties of Pyrolytic Carbon." Chemistry and Physics of Carbon, Vol. 5, p. 1, 1969.
11. Palmer, H. B. and Collis, C. F., "The Formation of Carbon from Gases." Chemistry and Physics of Carbon, Vol. 1, p. 265, 1965.
12. Fedoseev, D. V., Vnukov, S. P., and Derjaguin, B. V., "Physics -Chemical Theory of Graphite Growth from Hydrocarbons." Carbon, Vol. 17, p. 453, 1979.
13. Gebhardt, J. J., "Surface Effect in Pyrolytic Infiltration of Carbon Fiber Preforms." 14th Biennial Conference on Carbon, The Pennsylvania State University, p. 232, June 1979.